Enumeration of Spin-Space Groups:
Toward a Complete Description of Symmetries of Magnetic Orders

Yi Jiang,[1,2,3,*] Ziyin Song[1,2,*] Tiannian Zhu,[1,2] Zhong Fang,[1] Hongming Weng[1,4]
Zheng-Xin Liu[5,†] Jian Yang,[1,‡] and Chen Fang[1,4,6,§]

[1]*Beijing National Laboratory for Condensed Matter Physics, and Institute of Physics,*
Chinese Academy of Sciences, Beijing 100190, China
[2]*University of Chinese Academy of Sciences, Beijing 100049, China*
[3]*Donostia International Physics Center (DIPC), Paseo Manuel de Lardizábal. 20018,*
San Sebastián, Spain
[4]*Songshan Lake Materials Laboratory, Dongguan, Guangdong 523808, China*
[5]*Department of Physics, Renmin University, Beijing 100876, China*
[6]*Kavli Institute for Theoretical Sciences, Chinese Academy of Sciences, Beijing 100190, China*

Symmetries of three-dimensional periodic scalar fields are described by 230 space groups (SGs). Symmetries of three-dimensional periodic (pseudo)vector fields, however, are described by the spin-space groups (SSGs), which were initially used to describe the symmetries of magnetic orders. In SSGs, the real-space and spin degrees of freedom are unlocked in the sense that an operation could have different spatial and spin rotations. SSGs give a complete symmetry description of magnetic structures and have natural applications in the band theory of itinerary electrons in magnetically ordered systems with weak spin-orbit coupling. *Altermagnetism*, a concept raised recently that belongs to the symmetry-compensated collinear magnetic orders but has nonrelativistic spin plitting, is well described by SSGs. Because of the vast number and complicated group structures, SSGs have not yet been systematically enumerated. In this work, we exhaust SSGs based on the invariant subgroups of SGs, with spin operations constructed from three-dimensional (3D) real representations of the quotient groups for the invariant subgroups. For collinear and coplanar magnetic orders, the spin operations can be reduced into lower-dimensional real representations. As the number of SSGs is infinite, we consider only SSGs that describe magnetic unit cells up to 12 times crystal unit cells. We obtain 157 289 noncoplanar, 24 788 coplanar-noncollinear, and 1421 collinear SSGs. The enumerated SSGs are stored in an online database with a user-friendly interface. We develop an algorithm to identify SSGs for realistic materials and find SSGs for 1626 magnetic materials. We also discuss several potential applications of SSGs, including the representation theory, topological states protected by SSGs, structures of spin textures, and refinement of magnetic neutron diffraction patterns using SSGs. Our results serve as a solid starting point for further studies of symmetry and topology in magnetically ordered materials.

I. INTRODUCTION

Crystallography is a long-lived and vibrant field that studies the symmetries of crystalline materials. With the help of group theory, the symmetries of three-dimensional (3D) crystals are classified into 230 space groups (SGs) [1,2] when combining the translational symmetries with 32 3D crystallographic point groups (PGs). Theoretically, SGs describe the symmetries of any 3D periodic scalar fields, such as the crystal potential field $V(\mathbf{r})$.

Magnetism is another century-old realm, where magnetic materials are classified according to their various magnetic orders including ferromagnetic (FM), ferrimagnetic, anti-ferromagnetic (AFM), spiral magnetic, and even more complicated orders. In magnetic materials, the magnetic moments arrange into periodic 3D pseudovector fields in the spin space on top of the crystals formed by atoms in real space. The pseudovector field is of even parity under space inversion $\mathcal{P}$ and is odd under the time-reversal symmetry (TRS) $\mathcal{T}$.

---

*These authors contributed equally to this work.

†liuzxphys@ruc.edu.cn

‡yjbuptphy@gmail.com

§cfang@iphy.ac.cn

Historically, by combining TRS with 230 SGs, 1651 (double) Shubnikov magnetic space groups (MSGs) [2–8] were introduced in order to describe the symmetries of magnetic materials. Shubnikov MSGs are classified into four types. The 230 type-II Shubnikov SGs describe nonmagnetic materials, while the remaining 1421 of type I, III, and IV describe magnetic ones. In Shubnikov MSGs, the rotations of the magnetic moments are locked with the lattice operations. For instance, a C_{4z} symmetry operation stands for a $\pi/2$ rotation of the lattice along the z axis together with the rotation of the magnetic moments for the same angle $\pi/2$ along the z direction. In later discussion, we call the actions on the magnetic order as "spin operations."

MSGs, although widely used, fail to give a complete description of the symmetries of the magnetic moment fields. This is because there also exist symmetry operations that have unlocked real-space and spin rotations. Such enlarged groups were introduced as spin-space groups (SSGs) [9,10], which are the natural generalizations of Shubnikov MSGs and contain Shubnikov MSGs as a subset. For instance, a real-space C_{4z} rotation may accompany a C_{2z} spin rotation. In Fig. 1, we illustrate the difference between SGs, MSGs, and SSGs. In Fig. 1(a), we show an atomic configuration generated by a C_4 rotation, leading to a C_4-symmetric crystal field $V(\mathbf{r})$. In Fig. 1(b), a C_4-symmetric magnetic order is added to the atoms. We use the notation $\{R_s \| R_l\}$ to denote an operation with space rotation R_l (the space translation part omitted for simplicity) and spin rotation R_s. The MSG symmetry $\{C_4 \| C_4\}$ is used to describe the symmetry of the magnetic moment field $\mathbf{M}(\mathbf{r})$ in Fig. 1(b). In Fig. 1(c), a different magnetic order is shown, where the C_4-related atoms have
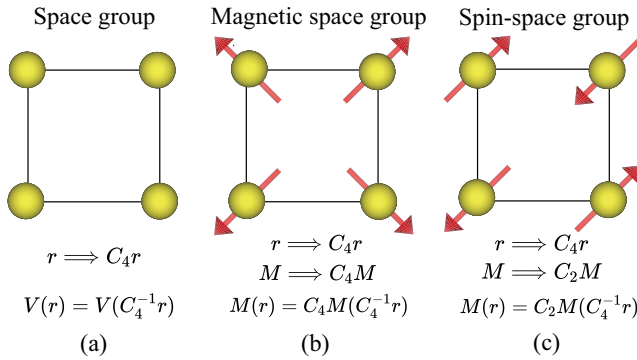

Space group	Magnetic space group	Spin-space group

$r \Longrightarrow C_4 r$ | $r \Longrightarrow C_4 r$ | $r \Longrightarrow C_4 r$
 | $M \Longrightarrow C_4 M$ | $M \Longrightarrow C_2 M$
$V(r) = V(C_4^{-1} r)$ | $M(r) = C_4 M(C_4^{-1} r)$ | $M(r) = C_2 M(C_4^{-1} r)$
(a) | (b) | (c)

FIG. 1. Illustration of SGs, MSGs, and SSGs. (a) A C_4-symmetric atomic configuration, generated by the SG operation C_4. (b) A magnetic order generated by the MSG operation $\{C_4 \| C_4\}$, where the real-space C_4 is accompanied by the same C_4 spin rotation. The notation $\{R_s \| R_l\}$ denotes an operation with space rotation R_l and spin rotation R_s. (c) A magnetic order generated by the SSG operation $\{C_2 \| C_4\}$, where the C_4 lattice rotation is accompanied by a C_2 spin rotation. MSGs, in which the spin and lattice rotation are locked, fail to give a complete symmetry description of this magnetic order.

C_2-rotated spin orientations, characterized by an SSG symmetry $\{C_2 \| C_4\}$, lying out of the scope of MSGs. This example demonstrates the incompleteness of MSGs in describing the symmetry of magnetic orders and the necessity for introducing SSGs.

SGs, Shubnikov MSGs, and SSGs also have important applications in describing the symmetries of electronic structures. Nonmagnetic periodic electronic structures characterized by a single-particle Hamiltonian $\hat{H} = (\hat{\mathbf{p}}^2/2m) + V(\mathbf{r})$ have their crystal potential field $V(\mathbf{r})$ respecting certain spatial symmetries, which form a (single) SG. The spin degree of freedom can be introduced in the Hamiltonian when the spin-orbit coupling (SOC) is present; i.e., a third term $(1/2m^2c^2)\nabla V(\mathbf{r}) \times \hat{\mathbf{p}} \cdot \hat{s}$ is added to the Hamiltonian, where $\hat{s}$ is the electron-spin operator. The symmetries of the (nonmagnetic) spinful Hamiltonians are described by double SGs together with the TRS, i.e., type-II (double) MSGs. The SOC term locks the spatial symmetries with the corresponding spin rotations in double MSGs. Only the lattice rotations associated with corresponding spin rotations are symmetries of the Hamiltonian. When the system is magnetically ordered, an effective "Zeeman term" $\mathbf{M}(\mathbf{r}) \cdot \hat{s}$ is generated. The effective Zeeman field may come from the mean-field decoupling of the electron interaction in the spin channel, where $\mathbf{M}(\mathbf{r})$ is the static mean field representing the magnetization, like in the spin-density-wave state. Alternatively, this Hamiltonian also describes the motion of an electron in the background of ordered, static magnetic moments, like in the Kondo lattice. The classifications of gapped topological states and unconventional quasiparticles protected by SGs [11–26] and MSGs [27–46] have been widely studied.

However, for itinerant electrons coming from light atoms or low angular momentum orbitals in magnetic materials, the SOC term is usually negligible or much smaller compared with the effective Zeeman term. Such systems are characterized by the single-particle Hamiltonian [47,48]

$$\hat{H} = \frac{\hat{\mathbf{p}}^2}{2m} + V(\mathbf{r}) + \mathbf{M}(\mathbf{r}) \cdot \hat{s}. \tag{1}$$

In these systems, the spin rotations are not necessarily always locked with lattice rotations due to the absence of the SOC, and the system may contain pure lattice rotation symmetries, pure spin rotation symmetries, and general symmetries with different lattice and spin rotations. Once the spin and the lattice operations are (partially) unlocked, the symmetries of the Hamiltonian form SSGs. Hence, spin-space groups not only describe the symmetries of magnetic structures, but also apply to electrons in magnetically ordered material having weak spin-orbit coupling and magnon Hamiltonian of spin systems [49] with weak Dzyaloshinskii-Moriya interactions.

It is worth mentioning that SSG can always be used to describe the symmetries of the magnetic structure of a

material, regardless of whether SOC is strong or not in the material. When SOC is non-negligible, the electronic structure of the material cannot be described by the SSG, and only MSG symmetries can be used. Nonetheless, SSG symmetries could serve as approximate symmetries for systems where SOC is weak or much smaller compared with the effective Zeeman term.

In 1977, Litvin tabulated 598 noncoplanar spin-point groups (SPGs) [50]. Very recently, 252 SPGs for coplanar and 90 SPGs for collinear magnetic orders have been listed [48]. A new concept, *altermagnetism*, has also been raised recently by the authors in Refs. [51–53], which describes a special type of collinear symmetry-compensated magnetic order that has nonrelativistic spin splitting or spin splitting with negligible SOC [54,55] in the Brillouin zone (BZ), breaking the Kramers degeneracy. The authors distinguished altermagnetic and AFM orders from symmetries using spin Laue point groups which are unlocked with the lattice point-group operations [51]. Therefore, altermagnetic materials [56–68] are naturally applicable systems of SSGs. An increasing number of experimental and theoretical studies on magnetic materials with weak SOC, among which many adopted the concept of SSGs, have been performed, including Mn_5Si_3 [56], RuO_2 [57–62], MnTe [63,64], $MnTe_2$ [69], $CoNb_3S_6$ [70,71], and the so-called "low-Z" antiferromagnetic compounds [72], together with many new quasiparticle types [47,48,70,71,73,74] being theoretically predicted, which can be realized only in SSGs.

Despite the wide applications of SSGs, the systematic enumeration of SSGs is mathematically incomplete as of today. Compared with spin-point groups, the enumeration of SSGs has the following difficulties: (i) The number of symmetry operations in an SSG is infinite due to the translation group. (ii) The number of SSGs is infinite, as the size of the magnetic unit cell could be arbitrary times of the original crystal unit cell, and even incommensurate magnetic orders exist. (iii) The spin rotations in SSGs could be noncrystallographic, such as a C_n rotation with arbitrary integer n. These difficulties hinder the enumeration of SSGs in the literature.

In this work, we enumerate SSGs systematically in order to give a complete symmetry description of all magnetic orders. We first exhaust invariant subgroups of 230 SGs and then compute the corresponding quotient groups that are isomorphic to point groups. The SSGs are constructed by assigning the 3D real representations of point groups as spin rotations to quotient group operations. 2D and 1D real representations are also enumerated to construct SSGs for coplanar and collinear magnetic orders. As the number of SSGs is infinite, we restrict our enumeration of SSGs with magnetic unit cells up to 12 times the crystal unit cells. We find 157 289 noncoplanar SSGs, 24 788 coplanar-noncollinear SSGs, and 1421 collinear SSGs. Especially for quotient groups isomorphic to crystallographic point groups, the size of the magnetic unit cell can be only within

12 times of the crystal unit cell and are, thus, exhausted in this work, which gives rise to 68 922 (noncoplanar) SSGs. The enumerated SSGs are stored in an online database [75] with a user-friendly interface. We also develop an algorithm to identify SSGs for magnetic materials, apply the algorithm to more than 2000 magnetic materials in Bilbao crystallographic server [6,76–79], and find the corresponding SSGs for 1626 commensurate magnetic materials without partial occupation.

The paper is organized as follows. In Sec. II, we give the formal definition of SSGs and the general framework for constructing SSGs. In Sec. III, we present the detailed algorithm for each step in enumerating SSGs. In Sec. IV, we summarize the enumeration results. In Sec. V, we use both pedagogical and realistic material examples to discuss the SSGs of magnetic structures. In Sec. VI, we discuss potential applications of SSGs. Finally, the paper is concluded in Sec. VII.

II. GENERAL FRAMEWORK

A. Definition of spin-space groups

We start with 230 SGs. An SG $\mathcal{G}$ has a 3D translation group

$$\boldsymbol{T} = \{\mathbf{R}_n = n_1\boldsymbol{a}_1 + n_2\boldsymbol{a}_2 + n_3\boldsymbol{a}_3, n_i \in \mathbb{Z}\} \quad (2)$$

as an invariant subgroup, where $\boldsymbol{a}_i$ ($i = 1, 2, 3$) are three primitive cell bases. $\mathcal{G}$ is represented as the coset decomposition

$$\mathcal{G} = \overset{n}{\underset{i=1}{\cup}} \{R_i|\boldsymbol{\tau}_i\}\boldsymbol{T}, \quad (3)$$

where $R_i \in O(3)$ is a point group operation and $\boldsymbol{\tau}_i \in \mathbb{R}^3$ is a translation, which is zero in symmorphic SGs and fractional under the bases of $\boldsymbol{T}$ in nonsymmorphic SGs. Denoting the collection of R_i as $P = \{R_i\}$, which is the point group of $\mathcal{G}$, then we have the quotient group $\mathcal{G}/\boldsymbol{T} \cong P$. For symmorphic SGs, P is a subgroup of $\mathcal{G}$, and $\mathcal{G} = \boldsymbol{T} \rtimes P$ is the semidirect product of the translation group and the PG. For nonsymmorphic SGs, P is no longer a subgroup of $\mathcal{G}$, and $\mathcal{G}$ is generally a group extension of $\boldsymbol{T}$ by P.

SGs can be used to describe the symmetry of a scalar field $V(\mathbf{r})$ if it is invariant under all lattice operations, where an SG operation acts on $V(\mathbf{r})$ in forms of

$$\{R_i|\boldsymbol{\tau}_i\}V(\mathbf{r}) = V(\{R_i|\boldsymbol{\tau}_i\}^{-1}\mathbf{r}). \quad (4)$$

However, to describe the complete symmetries of a periodic 3D pseudovector field (the magnetic moment field) $\mathbf{M}(\mathbf{r})$, one needs to define the operations that act on the pseudovector $\mathbf{M}$. A natural generalization is including the spin operations U_i, which yields the type-I MSG

$$\mathcal{G}^{(I)} = \bigcup_{i=1}^{n} \{U_i \| R_i|\boldsymbol{\tau}_i\}\boldsymbol{T}, \quad (5)$$

where $U_i = \det(R_i)R_i \in \mathrm{SO}(3)$ is the corresponding proper rotation matrix of R_i. The group element $\{U\|R|\boldsymbol{\tau}\}$ acts on the magnetic moment field $\mathbf{M}(\mathbf{r})$ as

$$\{U\|R|\boldsymbol{\tau}\}\mathbf{M}(\mathbf{r}) = \det(R)R\mathbf{M}(\{R|\boldsymbol{\tau}\}^{-1}\mathbf{r}). \quad (6)$$

By further including antiunitary TRS $\mathcal{T}$, one can obtain type-II, -III, and -IV MSGs which have the group structure $\mathcal{G}^{(\mathrm{II,III,IV})} = \mathcal{G} + m \cdot \mathcal{G}$, where $m = \mathcal{T}$, $g \cdot \mathcal{T}$, and $\boldsymbol{\tau} \cdot \mathcal{T}$ in type-II, -III, and -IV Shubnikov MSGs, respectively, with g being an SG symmetry with a nontrivial PG part and $\boldsymbol{\tau}$ a fractional translation. As $\mathcal{T}$ reverses $\mathbf{M}$, an antiunitary Shubnikov MSG element $\{U\|R|\boldsymbol{\tau}\}\mathcal{T}$ acts on $\mathbf{M}(\mathbf{r})$ as

$$\{U\|R|\boldsymbol{\tau}\}\mathcal{T}\mathbf{M}(\mathbf{r}) = -\det(R)R\mathbf{M}(\{R|\boldsymbol{\tau}\}^{-1}\mathbf{r}). \quad (7)$$

Here and later, we represent the action of time reversal $\mathcal{T}$ on the magnetic moment $\mathbf{M}$ as -1.

As last, when unlocking U_i from $\det(R_i)R_i$, we obtain the spin-space groups, which are noted as

$$\mathcal{G}^{(S)} = \overset{n}{\underset{i=1}{\cup}} \{U_i\|R_i|\boldsymbol{\tau}_i\}\boldsymbol{T}, \quad (8)$$

where $U_i \in \mathrm{O}(3)$. When $\det(U_i) = -1$, it is assumed that it contains TRS $\mathcal{T}$ and is antiunitary, i.e., $U_i \sim \det(U_i)U_i \cdot \mathcal{T}$. Under this assumption, we do not distinguish $U_i \in \mathrm{SO}(3) \times Z_2^T$ and $U_i \in \mathrm{O}(3)$, and the full operation of g reads

$$g = \begin{cases} \{U\|R_i|\boldsymbol{\tau}_i\}, & \text{if } \det(U) = +1, \\ \{-U\|R_i|\boldsymbol{\tau}_i\}\mathcal{T}, & \text{if } \det(U) = -1, \end{cases} \quad (9)$$

and an SSG operation $\{U\|R|\boldsymbol{\tau}\}$ acts on $\mathbf{M}(\mathbf{r})$ as

$$\{U\|R|\boldsymbol{\tau}\}\mathbf{M}(\mathbf{r}) = U\mathbf{M}(\{R|\boldsymbol{\tau}\}^{-1}\mathbf{r}). \quad (10)$$

To understand the group structure of SSG $\mathcal{G}^{(S)}$ defined in Eq. (8), it is convenient to introduce four key groups associated with $\mathcal{G}^{(S)}$ [10]: (i) the group $\mathcal{G}$ formed by the lattice parts $\{R|\boldsymbol{\tau}\}$; (ii) the group $\mathcal{S}$ formed by the spin parts $\{U\}$; (iii) the group H formed by pure-lattice symmetry operations $\{E\|R|\boldsymbol{\tau}\} \in \mathcal{G}^{(S)}$; (iv) the group $\mathcal{S}_0$ formed by pure-spin symmetry operations $\{U\|E|\mathbf{0}\} \in \mathcal{G}^{(S)}$, which is called the "spin-only group." (If U is an improper rotation with $\det U = -1$, then rigorously $\{U\|E|\mathbf{0}\}$ should be written as $\{U\|\mathcal{T}|\mathbf{0}\}$, since it acts nontrivially on the lattice wave vector. In this case, we still call $\{U\|\mathcal{T}|\mathbf{0}\}$ a "spin-only" operation.) From these definitions, it follows immediately that (a) both $\mathcal{G}$ and H are SGs; (b) H is an invariant subgroup of $\mathcal{G}$, i.e., $H \triangleleft \mathcal{G}$; and (c) $\mathcal{S}_0$ is an invariant subgroup of $\mathcal{S}$, i.e., $\mathcal{S}_0 \triangleleft \mathcal{S}$. According to the isomorphism theorem [10] (or Goursat's lemma [80]), the following quotient groups are isomorphic:

$$Q = \mathcal{G}/H \cong \mathcal{S}/\mathcal{S}_0. \quad (11)$$

For nonmagnetic systems, the spin-only group $\mathcal{S}_0 = \mathrm{O}(3)$, while for nontrivial magnetic orders, the pure-spin symmetries in $\mathcal{S}_0$ can appear in only two special types of magnetic orders [10].

(i) *Collinear magnetic orders, where* $\mathbf{M}(\mathbf{r}) = [0, 0, M_z(\mathbf{r})]$ *are set along the z direction without loss of generality.*—In this case, the spin-only group

$$\mathcal{S}_0 = \{C_\theta\|E|\mathbf{0}\} + \{M_x C_\theta\|E|\mathbf{0}\} \cong \mathrm{O}(2), \quad (12)$$

where C_θ denotes the rotation with an arbitrary angle θ along the z axis and M_x the mirror normal to the x axis. $M_x C_\theta$ generates all mirrors with mirror planes passing the z axis. Note that M_x, being improper, actually denotes the antiunitary operation $C_{2x}\mathcal{T}$. This spin-only group can also be written as $\mathcal{S}_0 = \mathrm{SO}(2) \rtimes \mathbb{Z}_2^{M_x} \cong \mathrm{O}(2)$, where $\mathrm{SO}(2)$ represents the continuous group from the C_θ rotation and $\mathbb{Z}_2^{M_x}$ is the $\mathbb{Z}_2$ group formed by the pure spin rotation M_x.

(ii) *Coplanar magnetic orders, where* $\mathbf{M}(\mathbf{r}) = [M_x(\mathbf{r}), M_y(\mathbf{r}), 0]$ *are set to lie on the z = 0 plane without loss of generality.*—In this case,

$$\mathcal{S}_0 = \mathbb{Z}_2^{M_z} = \{E, \{M_z\|E|\mathbf{0}\}\}, \quad (13)$$

where M_z denotes the mirror along the z axis. When an SSG $\mathcal{G}^{(S)}$ has a nontrivial spin-only group $\mathcal{S}_0$, $\mathcal{G}^{(S)}$ can always be decomposed into a direct product group by properly choosing the group element, i.e.,

$$\mathcal{G}^{(S)} = \mathcal{G}^{(S)\prime} \times \mathcal{S}_0, \quad (14)$$

where $\mathcal{G}^{(S)\prime} = \mathcal{G}^{(S)}/\mathcal{S}_0$ is "spin-only-free" and is still an SSG. In Supplemental Material Sec. VII [81], we give rigorous proof for the direct product group structure. For collinear and coplanar magnetic orders, the spin operations in $\mathcal{G}^{(S)\prime}$ can form only uniaxial point groups but not polyhedral point groups including T, T_h, T_d, O, and O_h [48], as the spin-only group $\mathcal{S}_0$ must be an invariant subgroup of $\mathcal{G}^{(S)}$.

We remark that one can also define 1651 single Shubnikov MSGs, where each operation has only a real-space part (combined with the TRS) but no spin part. Single Shubnikov MSGs are isomorphic to certain SSGs, as trivial spin rotations can be assigned to each spatial operation.

B. Construction of spin-space groups

In this work, we first construct SSGs with trivial spin-only groups $\mathcal{S}_0 = \{E\}$ which describe the symmetries of general magnetic orders. For collinear and coplanar magnetic orders, the spin-only group $\mathcal{S}_0$ has group structures shown in Eqs. (12) and (13) with the whole SSG being a direct product group of Eq. (14), and we construct the spin-only-free groups $\mathcal{G}^{(S)\prime}$ for them.

To construct SSGs, first notice that the pure-lattice symmetries in an SSG $\mathcal{G}^{(S)}$, i.e.,

$$H = \bigcup_i \{E \| R_i | \tau_i\} \boldsymbol{T}, \tag{15}$$

form an invariant subgroup of $\mathcal{G}^{(S)}$. The quotient group $Q = \mathcal{G}/H$ is a finite group and must be isomorphic to a subgroup of O(3), i.e., a point group. By assuming the spin-only group $\mathcal{S}_0$ is trivial, Q is isomorphic to the group formed by spin rotations:

$$Q = \mathcal{G}^{(S)}/H \cong \{U_i\}. \tag{16}$$

This relation gives insight into how to construct SSGs, as shown in the following.

For a given SG $\mathcal{G}$ with translation group $\boldsymbol{T}$ and PG P, assume $H \lhd \mathcal{G}$ is an invariant subgroup of $\mathcal{G}$, with $\boldsymbol{T}_H \lhd \boldsymbol{T}$ and $P_H \lhd P$. Denote the translational quotient group as $Q_T = \boldsymbol{T}/\boldsymbol{T}_H$ and point quotient group $Q_P = P/P_H$. The elements of $Q = \mathcal{G}/H$ are generated from the set products of Q_T and Q_P, where the rotations from Q_P have to recover their possible fractional translation parts τ in nonsymmorphic $\mathcal{G}$. As Q_T is an invariant subgroup of Q, the following short exact sequence holds:

$$\{E\} \to Q_T \xrightarrow{i} Q \xrightarrow{\pi} Q_P \to \{E\}, \tag{17}$$

where i maps Q_T to Q and π is surjection of Q onto Q_P, which induces an isomorphism

$$Q_P \cong Q/Q_T;$$

namely, Q is a group extension of Q_T by Q_P. If Q_P is also a subgroup of Q (which is not always the case), the group extension becomes a semidirect product $Q = Q_T \rtimes Q_P$.

Choose the representatives of the cosets in $\mathcal{G}$ with respect to its invariant subgroup H as $q_\alpha = \{R_\alpha | t_\alpha\}$, such that $\mathcal{G} = \bigcup_\alpha q_\alpha H$, where $R_\alpha \in Q$ is a PG operation and $t_\alpha = \tau_\alpha + \boldsymbol{R}_n$ is the original translation part τ_α associated with R_α plus a possible lattice translation. Assume Q has a

3D real representation D, with representation matrix $D(q_\alpha) = U_\alpha \in O(3)$. Then, an SSG $\mathcal{G}^{(S)}$ is constructed by

$$\mathcal{G}^{(S)} = \bigcup_\alpha \{U_\alpha \| R_\alpha | t_\alpha\} H, \tag{18}$$

where U_α denotes the rotation in spin space and operations in H are assigned with trivial spin rotations. The algorithm is schematically illustrated in Fig. 2.

For magnetic orders with nontrivial spin-only group $\mathcal{S}_0$, the general construction in Eq. (18) is applicable, but the existence of spin-only groups leads to additional equivalence relations between SSGs, and the construction of their corresponding SSGs can be simplified.

In the enumeration of SSGs, the involvement of a nontrivial spin-only group $\mathcal{S}_0$ effectively reduces the dimensionality of the spin space to be considered due to the imposed equivalence relations. For the three types of SSGs that have nontrivial $\mathcal{S}_0$, i.e., nonmagnetic, collinear, and coplanar, this dimensionality reduction allows us to focus solely on 0D, 1D, and 2D representations, respectively. As a result, this refinement in the enumeration process simplifies the procedure by limiting it to lower-dimensional representations, thereby reducing the breadth of groups that necessitate consideration.

For the nonmagnetic case, the spin-only group $\mathcal{S}_0 = O(3)$, and a spin-only-free group $\mathcal{G}^{(S)'} = \mathcal{G}^{(S)}/\mathcal{S}_0$ contains only pure-lattice operations as spin operations can be absorbed into $\mathcal{S}_0$ and is, thus, equivalent to one of the SG $\mathcal{G}$; hence, $\mathcal{G}^{(S)} = \mathcal{G} \times \mathcal{S}_0$. Thus, there are 230 inequivalent SSGs for nonmagnetic orders, i.e., 230 SGs. Mathematically, the trivial real representation is used to construct all spin operations in Eq. (18), i.e., $U_\alpha \equiv E$.

For collinear magnetic orders with $\mathbf{M}(\mathbf{r}) = [0, 0, M_z(\mathbf{r})]$, we have $\mathcal{S}_0 \cong O(2)$. There are two possibilities for the group $\mathcal{G}^{(S)}$, namely, $\mathcal{G}^{(S)} \cong O(2)$ or $\mathcal{G}^{(S)} \cong O(2) \times Z_2^T$; then, the quotient group $Q = \mathcal{G}^{(S)}/\mathcal{S}_0$ is $Q \cong C_1 = \{E\}$ and $Q \cong C_s = \{E, M_z\}$ (in the latter case, C_s has an equivalent replacement $Z_2^T = \{E, \mathcal{T}\}$), respectively. A spin-only-free group $\mathcal{G}^{(S)'} = \mathcal{G}^{(S)}/\mathcal{S}_0$ can be constructed from Eq. (18) where U_α is a 1D real representations of Q, i.e.,

Step 2

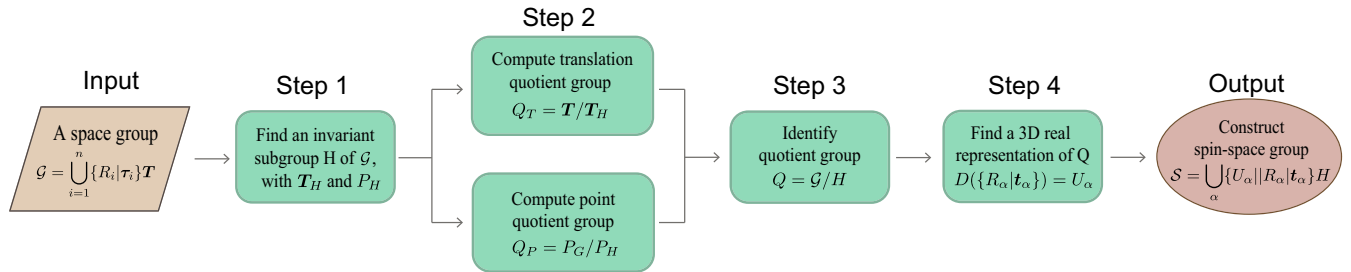| Input | Step 1 | Compute translation quotient group $Q_T = \boldsymbol{T}/\boldsymbol{T}_H$ | Step 3 | Step 4 | Output |

FIG. 2. Flowchart of the algorithm for constructing spin-space groups. We use $\{R_\alpha | t_\alpha\}$ to represent operations in the quotient group Q, where the translation part $t_\alpha = \tau_\alpha + \boldsymbol{R}_n$ is the original translation part τ_α associated with R_α in $\mathcal{G}$ plus a possible lattice translation. For collinear (coplanar) SSGs, 1D (2D) real representations are used.

$D(q_\alpha) = \pm 1$, direct summed with two trivial representations [such that $U_\alpha \in O(3)$]. The SSGs for collinear magnetic orders can be further classified into three types.

(1) When $Q \cong C_1$, then $\mathcal{G}^{(S)'} = \mathcal{G}$, which gives 230 collinear SSGs. These SSGs describe FM orders with spin splitting.

(2) When $Q \cong T/T_H \cong C_s$ (or, equivalently, $Q \cong Z_2^T$), then $\mathcal{G}^{(S)'} = H + \{M_z \| \mathcal{T} | 0, 0, 1\} H$ (or, equivalently, $\mathcal{G}^{(S)'} = H + \{\mathcal{T} \| \mathcal{T} | 0, 0, 1\} H$). In this case, one also has $g = \{C_{2y} \| E | 0, 0, 1\} \in \mathcal{G}^{(S)}$ (or $\{\mathcal{T} \| \mathcal{T} | 0, 0, 1\} \in \mathcal{G}^{(S)}$), which leads to spin degeneracy over the BZ. These SSGs describe conventional AFM with non-relativistic spin degeneracy.

(3) When $Q \cong P/P_H \cong C_s$ (or, equivalently, $Q \cong Z_2^T$), then $\mathcal{G}^{(S)'} = H + \{M_z \| R\mathcal{T} | \tau\} H$ (or, equivalently, $\mathcal{G}^{(S)'} = H + \{\mathcal{T} \| R\mathcal{T} | \tau\} H$).

    (a) If $R = \mathcal{P}$ is the real-space inversion, then there exists a combined spatial inversion and time-reversal symmetry $\mathcal{PT}$ which leads to spin degeneracy (both nonrelativistic and relativistic) in the whole BZ. These SSGs also describe conventional AFM orders.

    (b) If R is not the real-space inversion, then there is no symmetry that can protect spin degeneracy over the whole BZ. These SSGs describe the so-called "altermagnetism" [51–53] that differs from the conventional collinear AFM orders by the nonrelativistic spin splitting together with many other differences in transport properties.

For coplanar magnetic orders with $\mathbf{M}(\mathbf{r}) = [M_x(\mathbf{r}), M_y(\mathbf{r}), 0]$, $\mathcal{S}_0 = \mathbb{Z}_2^{M_z}$. The group $\mathcal{G}^{(S)}$ can be either C_{2v} (main axis x) or C_{nh}, D_{nh} (main axis z), with the quotient group $Q = \mathcal{G}^{(S)}/\mathcal{S}_0$ isomorphic to C_s (main axis x), C_n, C_{nv} (main axis z), respectively. The operations in the spin-only-free group $\mathcal{G}^{(S)'}$ are constructed by a direct sum of a 2D real representation in the xy plane and one trivial representation in the z direction.

Using this algorithm, we first compute the invariant subgroups in 230 SGs and then derive the quotient groups and their 3D real representations. SSGs are constructed by assigning the 3D real representation to the quotient group elements as spin operations. In the following section, we give more detailed descriptions of each step.

III. DETAILED ALGORITHM

Before diving into the details of the enumeration of SSGs, it is instructive to consider how to enumerate 230 SGs. Suppose we have 32 crystallographic point groups and 14 Bravais lattices, the latter of which give the bases of translation group T. Then, constructing SGs is a group extension problem, i.e., an extension of the translation group T by the PG P.

In practice, the problem can be transformed into solving a set of linear equations. For a given PG P and translation group T, suppose the SG $\mathcal{G}$ constructed from them has elements $g = \{p | \boldsymbol{\tau}_p\}$, where $p \in P$ and $\boldsymbol{\tau}_p$ are the translational part to be solved. The following two equations must be satisfied for $\mathcal{G}$ to form a group:

$$pT = T \quad \forall \ p \in P,$$
$$\boldsymbol{\tau}_{p_1 p_2} = \boldsymbol{\tau}_{p_1} + p_1 \boldsymbol{\tau}_{p_2} \quad \text{mod } T \quad \forall \ p_1, p_2 \in P. \quad (19)$$

The first equation means T is invariant under all $p \in P$, which is equivalent to requiring all $p \in P$ are integer $O(3)$ matrices in the primitive bases. The second equation is nothing but the group multiplication rule in $\mathcal{G}$. By iterating over 32 point groups and their compatible Bravais lattices, these equations can be solved to give all possible SGs.

However, the resultant number of SGs is larger than 230, as many of them are equivalent. To obtain inequivalent SGs, one has to define the equivalent relation between SGs. Two SGs $\mathcal{G}_1$ and $\mathcal{G}_2$ are equivalent if there exists a coordinate transformation $W = \{A | t\}$, where $A \in \mathrm{SL}(3, \mathbb{Z})$ and $t \in \mathbb{R}^3$, such that

$$\mathcal{G}_1 = W \mathcal{G}_2 W^{-1}. \quad (20)$$

Notice that the length of the primitive cell bases in T and the angles between them are inessential in defining equivalent SGs. In the literature [1], there are 230 (crystallographic) space-group types if requiring $A \in \mathrm{SL}(3, \mathbb{Z})$ and 219 affine space-group types if $A \in \mathrm{GL}(3, \mathbb{Z})$.

A. Subgroups of space groups

Assume an SG $\mathcal{G}$ with PG P and translational group T has a subgroup H with sub-PG P_H and subtranslational group T_H. Define the t index $I_t = |P/P_H|$ and k index $I_k = |T/T_H|$, which denote the number of elements in the point and translation quotient group, respectively. Remark that, although both T and T_H are infinite Abelian groups, their quotient group is a finite group when the translation basis in T and T_H are commensurate, determined by the transformation between their translation basis, i.e., original unit cell basis given by T and the supercell basis given by T_H. In the literature [1], subgroups with $I_t \geq 2$ and $I_k = 1$ are called the *translationengleiche* subgroup (t subgroup), and subgroups with $I_t = 1$ and $I_k \geq 2$ are called the *klassengleiche* subgroup (k subgroup) [82].

We then consider how to enumerate subgroups of SGs. When $I_k \geq 2$, i.e., the translational bases of the subgroup are enlarged and form a supercell, the subgroup is more complicated, because an integer translation in $\mathcal{G}$ may become a fractional translation in H, which means the subgroup of a symmorphic SG could be a nonsymmorphic SG.

Denote the elements of H as $\{\tilde{p} | \tilde{\boldsymbol{\tau}}_{\tilde{p}} + \tilde{\boldsymbol{t}}\}$, where $\tilde{\boldsymbol{t}} \in T_H$ is a lattice translation and $\tilde{\boldsymbol{\tau}}_{\tilde{p}}$ is the fractional translation associated with $\tilde{p}$ in $\mathcal{G}$, written in the bases of T_H. Symbols

with a tilde always represent operations in H. The fractional translation in H can be expressed as $\tilde{\boldsymbol{\tau}}_{\tilde{p}} = \boldsymbol{\tau}_{\tilde{p}} + \boldsymbol{t}_{\tilde{p}}$, where $\boldsymbol{\tau}_{\tilde{p}}$ is the fractional translation associated with $\tilde{p}$ in T and $\boldsymbol{t}_{\tilde{p}}$ a lattice translation in T. The following equations must be satisfied for H to form a subgroup of $\mathcal{G}$:

$$\tilde{p}\boldsymbol{T}_H = \boldsymbol{T}_H,$$

$$\boldsymbol{\tau}_{\tilde{p}_1} + \tilde{p}_1\boldsymbol{\tau}_{\tilde{p}_2} - \boldsymbol{\tau}_{\tilde{p}_1\tilde{p}_2} = w(\tilde{p}_1, \tilde{p}_2) \mod \boldsymbol{T}_H, \quad (21)$$

$\forall\ \tilde{p}, \tilde{p}_1, \tilde{p}_2 \in P_H$, where $w(p_1, p_2) = \boldsymbol{\tau}_{p_1 p_2} - \boldsymbol{\tau}_{p_1} - p_1\boldsymbol{\tau}_{p_2}$. The first equation requires the translation group to be invariant under P_H, and the second equation is the multiplication rule that the translation part of each element must satisfy in the subgroup. The second equation can be reformulated as a modular linear equation $M \cdot v = w \mod \boldsymbol{T}_H$, where v has the dimension $3N_H$ and M has dimension $3N_H N_H \times 3N_H$, with N_H being the number of elements in P_H. The Smith normal form can be adopted to solve the modular equation, the details of which can be found in Supplemental Material Sec. I [81].

In practice, we first find all possible P_H and $\boldsymbol{T}_H$ of given I_t and I_k and then solve Eq. (21) to obtain all possible subgroups. $\boldsymbol{T}_H$ is generated by a supercell matrix $S = (s_1, s_2, s_3) \in \mathrm{GL}(3, \mathbb{Z})$ with $\det = I_k$, where s_i denotes a primitive basis, which consists of the integer combination coefficients of the primitive bases of T.

B. Invariant subgroups of space groups

For an invariant subgroup $H \triangleleft \mathcal{G}$, the invariant condition, i.e., $gHg^{-1} = H$, $\forall\ g \in \mathcal{G}$, must be satisfied apart from Eq. (21). This leads to the following equations:

$$p\boldsymbol{T}_H = \boldsymbol{T}_H,$$

$$\tilde{p}t - t = 0 \mod \boldsymbol{T}_H,$$

$$pt_{\tilde{p}} - t_{p\tilde{p}p^{-1}} = w(p, \tilde{p}) - w(p\tilde{p}p^{-1}, p) \mod \boldsymbol{T}_H, \quad (22)$$

$\forall\ \tilde{p} \in P_H, p \in P, t \in T$, where $w(p, \tilde{p})$ is defined similarly as in Eq. (21).

In practice, the second equation in Eq. (22) can be transformed into another modular linear equation $M' \cdot v = w' \mod \boldsymbol{T}_H$, where v has dimension $3N_H$ and M' has dimension $3N_{\mathcal{G}} N_H \times 3N_H$, with $N_{\mathcal{G}}$ and N_H being the number of elements in P and P_H, respectively. Each subgroup is checked using Eq. (22) to determine if it is an invariant subgroup. In this way, we obtain all invariant subgroups of SGs within a given supercell range.

C. Quotient groups

Given an invariant subgroup H of $\mathcal{G}$, the quotient group $Q = \mathcal{G}/H$ can be computed by first computing the translation quotient group $Q_T = T/\boldsymbol{T}_H$ and point quotient group $Q_P = P/P_H$.

The translation quotient group Q_T is a finite Abelian group of the structure $\mathbb{Z}_{n_1} \times \mathbb{Z}_{n_2} \times \mathbb{Z}_{n_3}$, where $n_1 n_2 n_3 = I_k$ is the supercell k index. The point quotient group Q_P is obtained from the coset representatives of P_H in P. The whole quotient group Q is a finite group, with elements being the set product of Q_T and Q_P, where the rotations from Q_P have to recover their possible fractional translation parts $\boldsymbol{\tau}$ in nonsymmorphic $\mathcal{G}$. The group structure of Q is determined by both $\mathcal{G}$ and H, which is the group extension of Q_T by Q_P.

We compute the multiplication table of Q and then identify the isomorphic abstract group. An algorithm to obtain isomorphism between finite groups is given in Supplemental Material Sec. II [81].

D. 3D real representations of the quotient group

The 3D real (unitary) representations of the quotient group can be used to construct SSGs. This is because the spin operations belong to O(3), and the representation matrix of a 3D real representation can always be transformed into a O(3) matrix. A finite group with 3D real (unitary faithful) representations must be isomorphic to a PG. Thus, we consider the quotient groups that are isomorphic to point groups, either crystallographic or noncrystallographic.

Point groups are classified into the following abstract point groups that are not isomorphic to each other: $C_n(n \in \mathbb{Z})$, $C_{nh}(n \in 2\mathbb{Z})$, $D_n(n \in \mathbb{Z}, n \geq 3)$, $D_{nh}(n \in 2\mathbb{Z})$, T, O, I, T_h, O_h, and I_h. The equivalent relations between point groups are summarized in Supplemental Material Sec. III [81]. The irreducible representations (IRREPs) of 32 crystallographic point groups are tabulated in Ref. [83], and IRREPs of noncrystallographic point groups can be found in *Mathematica* [84].

IRREPs of a finite group $\mathcal{G}$ can be classified into three types, i.e., real, pseudoreal, and complex [2]. 3D real representations are constructed from IRREPs of each abstract PG, which have three possible constructions:

  (i) from three 1D IRREPs, if all three 1D IRREPs are real or one of them is real and the other two are complex and conjugated;
  (ii) from a 1D and a 2D real IRREP;
  (iii) directly from a 3D real IRREP.

Moreover, we require that the 3D real representations are faithful, i.e., only the identity element in the PG has the identity representation matrix. This is because, otherwise, the corresponding SSG can also be constructed using a larger invariant subgroup, extended by the elements with the identity representation matrix.

E. Equivalent SSGs

To obtain the correct number of inequivalent SSGs, equivalent relation between SSGs must be defined. There are three levels of equivalence, i.e., equivalent supercells (translation subgroups), equivalent (invariant)

subgroups, and equivalent 3D real representations of the quotient groups.

Before moving on to the formal definition, we first give an example to gain some insights into the problem of equivalence. Consider SG 16 $P222$, which has C_{2x}, C_{2y}, and C_{2z} rotations. For a system with $P222$ symmetry, there is some arbitrariness in choosing three coordinate axes. For example, one can permute the x, y, z axis to the y, z, x axis or change the x and y axis to y and $-x$ axis, respectively. These two coordinate transformations can be represented by $C_{3,111}$ and C_{4z}. Using them as two generators, a transformation group of point group O can be generated. As three axes are equivalent under $C_{3,111}$, one can choose C_{2y} rotation to form a subgroup $P2_y$, and the other two subgroups $P2_x$ and $P2_z$ are equivalent to $P2_y$. Also, a n-fold supercell along any axis is equivalent. This example shows the importance of finding the transformations that leave the SG invariant, which can be described by the automorphism group of the SG.

For a given SG $\mathcal{G}$, its automorphism group, which is the set of coordinate transformations that leave $\mathcal{G}$ invariant, i.e., $\text{Auto}(\mathcal{G}) = \{W = \{A|t\}|A \in \text{SL}(3,\mathbb{Z}), t \in \mathbb{R}^3\}$ such that

$$W\mathcal{G}W^{-1} = \mathcal{G}. \tag{23}$$

Here, $A \in \text{SL}(3,\mathbb{Z})$ is a recombination of three coordinate bases that must have $\det(A) = 1$ such that the volume and chirality of the unit cell are unchanged. $t \in \mathbb{R}^3$ is a shift of the origin point, which can take an infinite number of values for a given A. Notice that the ordering of operations in $\mathcal{G}$ under W may change, but their matrix forms must remain unchanged. The automorphism groups of SGs are summarized in Supplemental Material Sec. IV [81]. We remark that, for the triclinic and monoclinic crystal systems, the number of automorphisms with different rotation parts is infinite, while the number for other crystal systems is finite.

The equivalence between supercells is defined as follows. For two supercells S_1 and S_2 of an SG $\mathcal{G}$, where S_i is a 3×3 matrix with each column being a basis vector of the supercell, they are equivalent if there exists an automorphism $W = \{A|t\}$ of $\mathcal{G}$ and an elementary column transformation C with $\det(C) = 1$, such that

$$S_1 = AS_2C. \tag{24}$$

C serves as a recombination of bases which is necessary.

After obtaining inequivalent supercells, we then define equivalent (invariant) subgroups under a given supercell. Two subgroups H_1 and H_2 of a given supercell S of SG $\mathcal{G}$ are equivalent if there exists an automorphism $W = \{A|t\}$ of $\mathcal{G}$ such that

$$WH_1W^{-1} = H_2, \qquad ASC = S, \tag{25}$$

where C is an elementary column transformation with $\det(C) = 1$ and the second equation means that the supercell S is invariant under the automorphism or, equivalently, the automorphism A^{-1} is an integer matrix in the supercell, i.e., $C = S^{-1}A^{-1}S \in \text{SL}(3,\mathbb{Z})$.

For a given invariant subgroup H with supercell T_H of SG $\mathcal{G}$, consider two 3D real representations D_1 and D_2 of the quotient group Q. We use the notation $(Q|D)$ to explicitly show the mapping from Q to D. $(Q|D_1)$ and $(Q|D_2)$ are equivalent if there exists an automorphism $W = \{A|t\}$ of $\mathcal{G}$, such that H together with T_H are invariant under W, i.e., $WHW^{-1} = H$, $WT_HC = T_H$ (C is an elementary column transformation), and

$$(WQW^{-1}|D_1) \cong (Q|D_2), \tag{26}$$

where W acts only on the quotient group operations and $\cong$ means the transformed representation $(WQW^{-1}|D_1)$ is equivalent to $(Q|D_2)$, which does not require their representation matrix to be the same, but only their characters to be the same.

Based on the aforementioned equivalent relations, we are able to find all inequivalent invariant subgroups and 3D real representations of the quotient group. The SSGs constructed from them are, thus, all inequivalent. We leave more technical details to Supplemental Material Sec. V [81].

IV. RESULTS

A. Summary of enumeration results

Using the algorithm introduced in Sec. III, we obtain a vast number of SSGs. There are

(i) 331 661 subgroups with k index $I_k \leq 12$ and 2443 subgroups with $I_k = 1$ (i.e., without a supercell).

(ii) 27 197 invariant subgroups with k index $I_k \leq 12$ and 1708 invariant subgroups with $I_k = 1$.

(iii) 10 439 quotient groups isomorphic to crystallographic point groups and 68 922 SSGs constructed by their 3D real representations.

(iv) 7994 quotient groups isomorphic to noncrystallographic point groups with maximal operation rank less equal than 24 and 88 367 SSGs constructed from them.

(v) The total number of inequivalent SSGs with $I_k = 1$ is 8505.

(vi) The total number of inequivalent noncoplanar SSGs is 157 289.

(vii) The number of inequivalent collinear SSGs is 1421, and the number of coplanar-noncollinear SSGs is 24 788.

We use the following serial number to label (noncoplanar) SSGs:

$$N_{\text{SG}}.I_k.I_t.N_{\text{3Drep}}, \tag{27}$$

where N_{SG} is the SG number, $I_k = |T_\mathcal{G}/T_H|$ is the supercell k index, $I_t = |P_\mathcal{G}/P_H|$ is the t index, and N_{3Drep} denotes the Nth 3D representation of given I_k and I_t. For collinear and coplanar SSGs, we add extra $.L$ and $.P$ to the SSG label, i.e., $N_{SG}.I_k.I_t.N_{1Drep}.L$ for collinear SSGs and $N_{SG}.I_k.I_t.N_{2Drep}.P$ for coplanar SSGs.

In order to exhibit the vast number of SSGs, we develop a user-friendly online database [75], enabling easy searching of SSGs based on given information. On the search page, one can specify the desired SSG in the format $N_{SG}.I_k.I_t.N_{rep}(.L \text{ or } .P)$ or the first three numbers $N_{SG}.I_k.I_t$ which will retrieve all eligible SSGs. A side bar allows users to narrow down the search by selecting the space group number, SSG types, and equivalent quotient group label and specifying the range of I_k and I_t. On the Web site of each SSG, we give SSG operations in Q, the pure-lattice operations in H, and other basic information about the SSG.

In the following, we compare our results with the literature and summarize some general rules for the construction of SSGs.

B. Comparison with SPGs and MSGs

Litvin enumerated 598 SPGs in 1977 [50]. SPGs are constructed using PGs, which do not have translational symmetries. The automorphism group of a PG P is defined as $\text{Auto}(P) = \{A | A \in \text{SL}(3,\mathbb{R})\}$, which does not require A to be an integer matrix. For example, a $\pi/4$ rotation along the z axis is an automorphism of PG $D_4(422)$ but not an automorphism of SG $P422$.

For 32 symmorphic SGs that correspond to 32 PGs, we find 736 SSGs without considering supercells by restricting $I_k = 1$. Compared with 598 SPGs, there are six SGs, i.e., $P422$, $P4mm$, $P4/mmm$, $P622$, $P6mm$, and $P6/mmm$, that have extra SSGs, which all result from the difference in the definition of automorphism groups of SG and PG.

For 1651 Shubnikov MSGs, 230 type-II nonmagnetic SGs have time-reversal symmetry, which can be constructed using 230 SGs with spin-only groups $\mathcal{S}_0 = \text{O}(3)$.

230 type-I single Shubnikov MSGs can be constructed from 230 SGs by considering $I_k = 1$, $H = G$, and $Q = 1$; i.e., all symmetries have no spin rotation part. If we consider $I_k = 1$ and $H = P1$, then $Q = P_\mathcal{G}$. In this case, if $\mathcal{G}$ contains no symmetry with $\det = -1$, then the corresponding SSG is isomorphic to the corresponding type-I double Shubnikov MSGs. On the other hand, if $\mathcal{G}$ contains symmetries with $\det = -1$, then the SSG is isomorphic to certain type-III double Shubnikov MSGs.

674 type-III single Shubnikov MSGs can be constructed from 230 SGs by considering all index-2 invariant subgroups of SGs with $I_t = 2$ and $I_k = 1$. In this case, the quotient group $Q = \mathcal{G}/H \cong C_i$. The inversion symmetry assigned to the quotient group is equivalent to the TRS, and, thus, $\mathcal{G}^{(S)} \cong H + g \cdot \mathcal{T}H$.

517 type-IV single Shubnikov MSGs can be constructed from 230 SGs by considering all $I_k = 2$, $I_t = 1$ invariant subgroups, which have the quotient group $Q = \mathcal{G}/H \cong C_i$. The inversion symmetry is assigned to one translation, and $\mathcal{G}^{(S)} \cong H + \boldsymbol{\tau} \cdot \mathcal{T}H$. The resultant number of SSGs is exactly the same number of the type-IV Shubnikov MSGs under OG setting for each SG.

C. General rules for constructing quotient groups

Despite the vast number of SSGs, many of them have quotient group structures that can be exhausted for arbitrary supercell indexes I_k. In the following, we list several examples of such constructions of quotient groups, and a more detailed discussion can be found in Supplemental Material Sec. VI [81].

When the quotient group $Q \cong C_n$, the invariant subgroup H must satisfy $P/P_H \cong \mathbb{Z}_p$, $T/T_H \cong \mathbb{Z}_q$, where $pq = n$ and p and q are not necessarily mutually prime. For example, for $\mathcal{G} = P4_1$, $P_H = 1$, and $T/T_H \cong \mathbb{Z}_6$, with the supercell along the z direction, the quotient group $Q \cong C_{24}$ is generated by $\{C_{4z}|0,0,\frac{1}{4}+1\}$, which has rank 24.

When $Q \cong C_{nh}$, the invariant subgroup H could have the structure $P/P_H \cong C_2$, $T/T_H \cong \mathbb{Z}_n$, where $n \in \mathbb{Z}$, $n \geq 2$, and C_2 must commute with the generator of T/T_H. For example, for $\mathcal{G} = P2$, $P_H = 1$, $P/P_H = C_2$, and $T/T_H \cong \mathbb{Z}_n$, with the rotation and supercell both along the y direction, the quotient group $Q \cong C_{nh}$ is generated by $\{C_{2y}|\mathbf{0}\}$ and $\{E|0,1,0\}$.

When $Q \cong D_n$, the invariant subgroup H could also have the structure $P/P_H \cong C_2$, $T/T_H \cong \mathbb{Z}_n$, where $n \geq 3$, but C_2 must not commute with the generator of T/T_H. For example, for $\mathcal{G} = P\bar{1}$, $P_H = 1$, $P/P_H = C_i$, and $T/T_H \cong \mathbb{Z}_n$, with the supercell along the z direction, the quotient group $Q \cong D_n$ is generated by $\{E|0,0,1\}$ and $\{\mathcal{P}|\mathbf{0}\}$, which do not commute with each other.

D. Quotient groups isomorphic to crystallographic point groups

We claim that we exhaust all SSGs that have spin parts isomorphic to crystallographic point groups, with reasons given below.

The translation quotient group Q_T is a finite Abelian group. For abstract point groups, only the following are Abelian: $C_n \cong \mathbb{Z}_n$, $C_{nh}(n/m) \cong \mathbb{Z}_n \times \mathbb{Z}_2$, and $D_{2h}(mmm) \cong \mathbb{Z}_2 \times \mathbb{Z}_2 \times \mathbb{Z}_2$. This can be seen from the fact that a C_n rotation with $n > 2$ does not commute with rotations along other axes. Among these abstract point groups, only C_n ($n = 1, 2, 3, 4, 6$), C_{nh} ($n = 2, 4, 6$), and D_{2h} are crystallographic point groups.

As a result, to exhaust all quotient groups that are isomorphic to crystallographic point groups, we need only to consider the supercell of k index $I_k \in \{1, 2, 3, 4, 6, 8, 12\}$. Their isomorphisms are tabulated in Table I. Supercells

TABLE I. Translation quotient groups that are isomorphic to crystallographic point groups.

k index	Translation quotient group	Isomorphic PG
1	$\mathbb{Z}_1$	$C_1(1)$
2	$\mathbb{Z}_2$	$C_2(2)$
3	$\mathbb{Z}_3$	$C_3(3)$
4	$\mathbb{Z}_4$	$C_4(4)$
4	$\mathbb{Z}_2 \times \mathbb{Z}_2$	$C_{2h}(2/m)$
6	$\mathbb{Z}_6$	$C_6(6)$
8	$\mathbb{Z}_4 \times \mathbb{Z}_2$	$C_{4h}(4/m)$
8	$\mathbb{Z}_2 \times \mathbb{Z}_2 \times \mathbb{Z}_2$	$D_{2h}(mmm)$
12	$\mathbb{Z}_6 \times \mathbb{Z}_2$	$C_{6h}(6/m)$

with other k indexes have translation quotient groups that are not isomorphic to any crystallographic point groups and so are the whole quotient groups. This is because the translation quotient group is an invariant subgroup of the whole quotient group, and the whole quotient group cannot be isomorphic to a crystallographic PG if it has a subgroup that is not isomorphic to any crystallographic point groups. This means that, by considering all invariant subgroups of SGs with $I_k \leq 12$, we are able to find all SSGs with spin part isomorphic to crystallographic point groups.

E. SSGs for incommensurate magnetic orders

Our approach also applies to constructing the SSGs for incommensurate magnetic structures. For example, consider the simplest incommensurate spiral magnetic structure along the z direction. In this case, the translational quotient group $\boldsymbol{T}/\boldsymbol{T}_H$ is isomorphic to the noncrystallographic point group C_n with n going to infinity (i.e., $\boldsymbol{T}/\boldsymbol{T}_H \cong \mathbb{Z}$). The corresponding SSG is generated by the operation $\{C_{2\pi\alpha}\|E|\boldsymbol{a}_3\}$; i.e., the z-directional lattice translation $\boldsymbol{a}_3$ is accompanied by an incommensurate spin rotation $C_{2\pi\alpha}$, where α is an irrational number. We can approximate α as a rational number, i.e., $\alpha \approx (m/n)$, which leads to $|\boldsymbol{T}/\boldsymbol{T}| \approx \mathbb{Z}_n$. n will go to infinity when α is approximated more accurately.

An interesting question arises concerning why noncrystallographic operations could appear in periodic systems. The key lies in understanding that the noncrystallographic rotations are confined only to the spin part in SSGs. These rotations do not influence the $\boldsymbol{r}$ or $\boldsymbol{k}$ but exclusively act on the magnetic moments $\boldsymbol{M}(\boldsymbol{r})$ or spinor Bloch states $\psi_\sigma(\boldsymbol{k})$. This distinction allows for the incorporation of noncrystallographic symmetries within the periodic framework of SSGs.

We also discuss briefly the relation of SSGs with superspace groups [85,86]. Superspace groups are conventionally employed in the realm of incommensurate crystallography and are generalized later to magnetic systems [87]. In superspace groups, a basic (periodic) structure is described by an SG or an MSG, together with a modulation function $A_{\mu R}$ defined on atom μ in unit cell $\boldsymbol{R}$, which characterizes the atomic displacements (e.g., charge

density waves), the magnetic moments (e.g., spin density waves), fractional occupancy of atoms, or other possible local physical quantities. The modulation function $A_{\mu R}(x_4)$ has a variable $x_4 = \boldsymbol{q} \cdot (\boldsymbol{r}_\mu + \boldsymbol{R})$ with $\boldsymbol{q}$ being the propagation vector, either commensurate or incommensurate. x_4 is introduced as a higher dimension besides the three-dimensional real space and describes the aperiodicity of the system. Multiple propagation vectors are also supported in superspace groups.

Compared with (magnetic) superspace groups, SSGs are more powerful in describing complicated magnetic structures, where symmetries with unlocked spin and real-space rotations are allowed. This type of symmetry is uniquely described in SSGs. It is worth mentioning that SSGs inherently restrict to a single principal axis around which noncrystallographic spin rotations occur. Multiple principal axes of the noncrystallographic spin operations are not allowed in SSGs. This is because the noncrystallographic spin rotations are generated by the translation quotient group $\boldsymbol{T}/\boldsymbol{T}_H = \mathbb{Z}_{n_1} \times \mathbb{Z}_{n_2} \times \mathbb{Z}_{n_3}$, which is an Abelian group. Thus, the noncrystallographic spin operations assigned to the elements in $\boldsymbol{T}/\boldsymbol{T}_H$ must also commute, which means they share the same principal axis. For example, consider two SSG operations $g_1 = \{C_{mx}\|E|100\}$ and $g_2 = \{C_{ny}\|E|010\}$, with m, $n > 2$. A system with $g_{1,2}$ is enforced to be nonmagnetic because $g_1 g_2 \neq g_2 g_1$, which will generate a nontrivial spin-only group that enforces zero magnetization.

However, a single principal axis in the spin part does not necessarily indicate a single propagation vector in SSGs. An extra propagation vector could be given by the twofold spin operations perpendicular to the principal axis. For example, a SSG generated by $\{C_{nz}\|E|0,0,1\}$ and $\{M_z\|E|0,1,0\}$ ($n > 6$ is even) has propagation vector $Q_1 = [0,0,(1/n)]$, $Q_2 = (0,\frac{1}{2},0)$. Note that if n is odd, C_{nh} is isomorphic to C_{2n}, and a single propagation vector describes the corresponding magnetic order.

When the magnetic order is generated by two spin rotations along the same axis in two real-space directions, e.g., $\{C_{mz}\|E|1,0,0\}$ and $\{C_{nz}\|E|0,1,0\}$, they are described by a single propagation vector. This is because (i) when m and n are coprime, one can adopt a single generator with spin rotation $\{C_{mn,z}\|E|a,b,0\}$, together with a pure translation $\{E\|E|m,n,0\}$, where $an - bm = 1$ such that the unit cell volume is maintained; (ii) when m and n are not coprime but have a greatest common divider w, one can still find a new generator $\{C_{\frac{mn}{w},z}\|E|a,b,0\}$ together with $\{E\|E|(m/w),(n/w),0\}$, where $an - bm = w$ (i.e., the Bézout identity), such that the unit cell volume is maintained. However, we remark that if there are multiple propagation vectors along the same direction, the magnetic moments, in general, cannot have the same magnitude. SSGs cannot describe this type of magnetic structure, because the spin rotations in SSG are O(3) matrices that maintain the length of magnetic moments.

For incommensurate magnetic structures, they can be approximated by commensurate magnetic structures, and the discussion above still applies. Thus, we conclude that SSGs can effectively describe incommensurate magnetic structures using noncrystallographic spin operations, which have only a single principal axis resulting from the group structure of the noncrystallographic point groups. In this case, multiple propagation vectors are still allowed.

Both SSGs and superspace groups have their unique strengths and are useful in the realm of crystallography and magnetism. It is also possible to integrate SSGs in the superspace group formalism by replacing MSGs with SSGs for the basic periodic structure.

V. SSGS OF MAGNETIC STRUCTURES

In this section, we give several pedagogical examples to show the construction of SSGs.

A. Pedagogical examples

First, for each symmorphic SG, a special type of SSG can be constructed using invariant subgroups H with $I_t = 1$ and $I_k = n$, i.e., $P/P_H = 1$, $T/T_H = \mathbb{Z}_n$, and, thus, $Q \cong \mathbb{Z}_n$. Assume the n-fold supercell is along the z axis. Then, the SSG is generated by an n-fold operation:

$$\{C_n \| E | 001\}, \tag{28}$$

where E is the identity operation. This operation means a lattice translation in the z axis is accompanied by a C_n rotation in spin space, which can be used to describe the spiral magnetism. In Fig. 3(a), we show a possible spiral magnetic phase generated by $\{C_4 \| E | 001\}$.

Next, we show that different 3D real representations can construct different SSGs. As an example, consider SG 10 $P2/m$ and a trivial invariant subgroup H with $P_H = 1$, $T_H = T$. The quotient group $Q \cong C_{2h}$ has four real IRREPs $\Gamma_1^\pm$ and $\Gamma_2^\pm$, as shown in Table II. These IRREPs can be combined to form ten 3D real representations, as shown in Table III. Note that the ordering of the three 1D IRREPs in a 3D real representation is inessential, as it changes only the main axis of the equivalent PG, which corresponds to the main axis in spin space and can be chosen arbitrarily. These ten 3D real representations give ten inequivalent SSGs. For example, the SSG formed by $\Gamma_2^- \oplus \Gamma_1^- \oplus \Gamma_2^-$ has elements

$$\{E\|E|\mathbf{0}\}, \ \{C_{2y}\|C_{2y}|\mathbf{0}\}, \ \{\mathcal{P}\|\mathcal{P}|\mathbf{0}\}, \ \{M_y\|M_y|\mathbf{0}\}, \tag{29}$$

which is nothing but the double SG $P2/m$, with the real-space part and spin-space part being locked. The SSG formed by $\Gamma_1^- \oplus \Gamma_2^+ \oplus \Gamma_2^-$ has elements

$$\{E\|E|\mathbf{0}\}, \ \{C_{2x}\|C_{2y}|\mathbf{0}\}, \ \{C_{2y}\|\mathcal{P}|\mathbf{0}\}, \ \{C_{2z}\|M_y|\mathbf{0}\}, \tag{30}$$
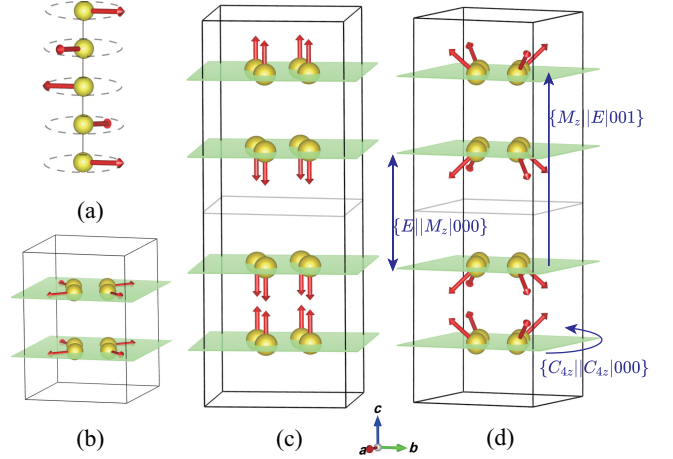

FIG. 3. Examples of magnetic orders and their spin-space groups. (a) A schematic show of spiral magnetic phase, where a lattice translation along the z axis is associated with a C_{4z} rotation in spin space, i.e., $\{C_{4z}\|E|001\}$. (b)–(d) Three possible magnetic orders generated from the same space group $P4/m$, where (b) is a coplanar order, (c) a collinear order, and (d) a general noncoplanar order, yielding SSGs 83.1.4.1.P, 83.2.1.1.L, and 83.2.4.1, respectively. In (d), we use blue arrows to denote three generators of the corresponding SSG 83.2.4.1, which includes a pure lattice operation $\{E\|M_z|000\}$, a spin-lattice locked operation $\{C_{4z}\|C_{4z}|000\}$, and a spin-lattice unlocked operation $\{M_z\|E|001\}$.

which is an SSG with real-space and spin-space parts unlocked.

As the third example, we exemplify the equivalent relation in SSGs. Consider SG 16 $P222$ and the trivial invariant subgroup as in the previous example, i.e., $Q \cong C_{2h}$. The ten 3D real representations, however, cannot form ten SSGs, because only three of them are inequivalent, i.e., $\Gamma_1^- \oplus \Gamma_2^+ \oplus \Gamma_2^- \cong D_2$, $\Gamma_1^+ \oplus \Gamma_1^- \oplus \Gamma_2^+ \cong C_{2v}$, and $\Gamma_1^- \oplus \Gamma_1^- \oplus \Gamma_2^+ \cong C_{2h}$. This is because the three C_2 rotations in $P222$ are equivalent, and the 3D real representations equivalent to the same PG are, thus, equivalent.

Lastly, we present a sophisticated example to demonstrate the construction of collinear, coplanar, and general noncoplanar SSGs from a single SG. Consider SG 83 $P4/m$, which can be generated using PG operations C_{4z} and M_z together with the three lattice translations. A generic atomic configuration of $P4/m$ is shown in Fig. 3(b), which has eight atoms in the unit cell. We first

TABLE II.   IRREPs of point group C_{2h}.

IRREP	E	C_2	$\mathcal{P}$	M
Γ_1^+	1	1	1	1
Γ_1^-	1	1	-1	-1
Γ_2^+	1	-1	1	-1
Γ_2^-	1	-1	-1	1

TABLE III. 3D real representations of point group C_{2h}, where the first column gives ten 3D real representations, the second to fifth columns give the representation matrix of each operation in C_{2h}, and the last column gives the equivalent PG of the 3D real representation.

3D real rep	E	C_2	$\mathcal{P}$	M	Eqv PG
$\Gamma_1^- \oplus \Gamma_2^+ \oplus \Gamma_2^-$	E	C_{2x}	C_{2y}	C_{2z}	D_2
$\Gamma_1^+ \oplus \Gamma_1^- \oplus \Gamma_2^+$	E	M_z	M_y	C_{2x}	C_{2v}
$\Gamma_1^+ \oplus \Gamma_1^- \oplus \Gamma_2^-$	E	M_z	C_{2x}	M_y	C_{2v}
$\Gamma_1^+ \oplus \Gamma_2^+ \oplus \Gamma_2^-$	E	C_{2x}	M_z	M_y	C_{2v}
$\Gamma_1^- \oplus \Gamma_1^- \oplus \Gamma_2^+$	E	M_z	C_{2z}	$\mathcal{P}$	C_{2h}
$\Gamma_1^- \oplus \Gamma_1^- \oplus \Gamma_2^-$	E	M_z	$\mathcal{P}$	C_{2z}	C_{2h}
$\Gamma_1^- \oplus \Gamma_2^+ \oplus \Gamma_2^+$	E	C_{2x}	M_x	$\mathcal{P}$	C_{2h}
$\Gamma_2^- \oplus \Gamma_1^- \oplus \Gamma_2^-$	E	C_{2y}	$\mathcal{P}$	M_y	C_{2h}
$\Gamma_2^+ \oplus \Gamma_2^+ \oplus \Gamma_2^-$	E	$\mathcal{P}$	M_z	C_{2z}	C_{2h}
$\Gamma_2^+ \oplus \Gamma_2^- \oplus \Gamma_2^-$	E	$\mathcal{P}$	C_{2x}	M_x	C_{2h}

consider a coplanar magnetic order as shown in Fig. 3(b), which has a pure spin reflection symmetry $\{M_z\|E|0\}$ owned by all coplanar orders. The magnetic moments of the four atoms on the same layer have C_{4z}-related directions, resulting in a spin-lattice locked operation $\{C_{4z}\|C_{4z}|0\}$. The atoms in two layers, however, share the same magnetic configuration, yielding a pure lattice symmetry $\{E\|M_z|0\}$. Thus, the coplanar SSG for this magnetic order is identified as SSG 83.1.4.1.P in our database.

We then consider a collinear magnetic order in Fig. 3(c), which has a twofold supercell along the z axis. The magnetic moments in two unit cells have reversed directions, leading to the $\{M_z\|E|001\}$ operation and the pure lattice operation $\{E\|M_z|0\}$. The spin-lattice locked operation $\{C_{4z}\|C_{4z}|0\}$ still exists, but, as the collinear order has spin-only operation $\{C_\theta\|E|0\}$ (θ being an arbitrary angle), the C_{4z} spin rotation can be omitted and leads to the pure lattice operation $\{E\|C_{4z}|0\}$. The invariant subgroup H formed by pure lattice operations is, thus, identified as $P4/m$ with a twofold supercell, leading to the collinear SSG 83.2.1.1.L.

As last, we consider a general noncoplanar order in Fig. 3(d), where we mark three generators of the SSG:

$$\{E\|M_z|0\}, \qquad \{C_{4z}\|C_{4z}|0\}, \qquad \{M_z\|E|001\}. \quad (31)$$

The generators of the translation group $\boldsymbol{T}$ are modified to $\{E|100\}$, $\{E|010\}$, and $\{E|002\}$. The corresponding SSG is identified as 83.2.4.1, which has the invariant subgroup H of pure lattice operations Pm with a twofold supercell along z. We emphasize that the SSG symmetries of this noncoplanar magnetic order are beyond MSGs. Within MSG, only the spin-lattice locked generator $\{C_{4z}\|C_{4z}|0\}$ remains, while the pure-lattice operation $\{E\|M_z|0\}$ and the spin-lattice unlocked operation $\{M_z\|E|001\}$ lie out of the scope of MSGs.

B. Realistic magnetic materials

In this work, we also develop an algorithm that can identify SSGs for realistic materials, with details given in Supplemental Material Sec. VIII [81]. We apply the algorithm to more than 2000 magnetic materials in the Bilbao crystallographic server [6,76–79] and find the corresponding SSGs for all 1626 commensurate magnetic materials without partial occupation, with results summarized in Supplemental Material Sec. VIII [81]. Before starting, we remark on the usage of SSG on magnetic materials: (i) SSGs serve as a fine-grained tool to describe symmetry and refine magnetic structures. (ii) SSGs describe the electronic structures of magnetic materials when SOC is negligible or weak compared to the spin splitting induced by the effective Zeeman term.

In the following, we present four examples of realistic materials with collinear, coplanar, and noncoplanar magnetism. We identify their corresponding SSGs and MSGs and show that SSGs have richer symmetries than MSGs.

Figure 4(a) depicts the collinear magnetic structure of RuO_2, a recently proposed typical *altermagnetic* material [57–62]. We take it as an example to demonstrate how to determine the SSG of collinear antiferromagnetic materials. RuO_2 has SG 136 $P4_2/mnm$ symmetry when magnetic moments are ignored. The pure lattice symmetry group H can be identified by considering the spin-up and
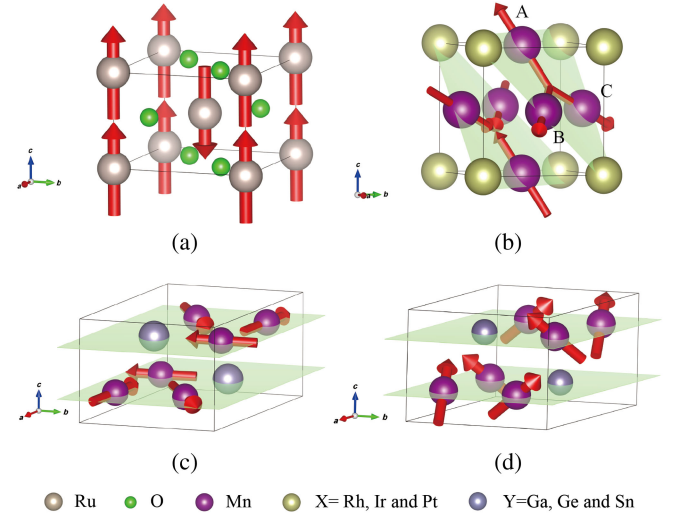

(a)   (b)

(c)   (d)

○ Ru   ● O   ● Mn   ○ X= Rh, Ir and Pt   ○ Y=Ga, Ge and Sn

FIG. 4. Realistic material examples of SSGs. (a) RuO_2 features a tetragonal lattice and a collinear antiferromagnetic order. (b) Mn_3X (X = Rh, Ir, and Pt) exhibits a face-centered cubic (fcc) crystal structure with a coplanar magnetic order where all magnetic moments reside on the (111) plane (highlighted in green). A, B, and C are used to label three Mn atoms located on the same plane. (c) Mn_3Y (Y = Ga, Ge, and Sn) has a hexagonal lattice where Mn atoms form two kagome layers and develop a coplanar magnetic order. (d) A deformed noncoplanar magnetic structure of (c), where the magnetic moments of Mn are rotated in the xy plane and acquire a z-directional component of equal magnitude.

spin-down atoms as different types of atoms, which is $Pmmm$ in RuO_2. The quotient group is then computed as C_4 with the generator $g = \{M_{001}\|4_{001}|\frac{1}{2},\frac{1}{2},\frac{1}{2}\}$. The collinear spin-only group $\mathcal{S}_0$ defined in Eq. (12) is also present. The SSG is, thus, determined as $136.1.2.6.L$ in our database. The MSG of RuO_2 is $136.499\ P4'_2/mnm'$, which forms a subgroup of the SSG. For example, $\{4_{001}\|4_{001}|\frac{1}{2},\frac{1}{2},\frac{1}{2}\}\cdot\mathcal{T} \sim \{4_{001}\cdot\mathcal{P}\|4_{001}|\frac{1}{2},\frac{1}{2},\frac{1}{2}\}$ in MSG can be obtained by combining g with the pure-spin operation $\{4_{001}^{-1}\|E|\mathbf{0}\}$.

Figures 4(b) and 4(c) display the coplanar magnetic structures of Mn_3X ($X =$ Rh, Ir, and Pt) and Mn_3Y ($Y =$ Ga, Ge, and Sn), respectively, which have been reported to exhibit strong anisotropic anomalous Hall effects and spin Hall effects [88,89]. In the following, we determine their corresponding SSGs separately.

As shown in Fig. 4(b), Mn_3X ($X =$ Rh, Ir, and Pt) has a face-centered cubic (fcc) crystal structure with three inequivalent face-centered Mn atoms having different magnetic orientations but all residing on the same (111) plane. The SG without considering magnetic moments is SG 221 $Pm\bar{3}m$. The pure lattice symmetry group H is determined to be $Pmmm$. The quotient group is, thus, isomorphic to C_{3v}, but the spin rotations are not straightforward to obtain. To clarify each SSG operation, we label three Mn atoms by A, B, and C in Fig. 4(b) and show the permutation of Mn atoms by the real-space rotations in Table IV. The spin rotations can then be determined by comparing the orientations of magnetic moments. For example, the real-space 2_{110} acts on Mn atoms as

$$2_{110}r_A = r_A, \qquad 2_{110}r_B = r_C, \qquad 2_{110}r_C = r_B. \qquad (32)$$

The accompanied spin operation should also switch the magnetic moments at B and C while leaving A unchanged, which is identified as $M_{1\bar{1}0}$ with the mirror plane perpendicular to the line connecting B and C. The SSG operation $\{3_{111}\|3_{111}\}$ can be identified similarly. The SSG

TABLE IV. Elements of the quotient group of $221.1.6.1.P$, i.e., symmetries of the magnetic structure in Fig. 4(b). The first column is the real-space operations, the second to fourth columns the permutation of positions A $(\frac{1}{2},\frac{1}{2},1)$, B $(1,\frac{1}{2},\frac{1}{2})$, and C $(\frac{1}{2},1,\frac{1}{2})$ under these operations, and the last column the corresponding spin operations.

Real-space operation	A	B	C	Spin operation
E	A	B	C	E
3_{111}	B	C	A	3_{111}
3_{111}^{-1}	C	A	B	3_{111}^{-1}
2_{110}	A	C	B	$M_{1\bar{1}0}$
4_{100}	C	B	A	$M_{01\bar{1}}$
4_{010}	B	A	C	$M_{10\bar{1}}$

is then determined as $221.1.6.1.P$ in the database, with all SG 221 operations maintained by assigning proper spin rotations. The MSG of Mn_3X is $166.101R\bar{3}m'$, with the main C_3 axis along (111). Two generators of SG 221 are broken in this MSG, i.e., 4_{100} and M_{100}, with the former having an unlocked spin rotation, i.e., $\{M_{01\bar{1}}\|4_{100}\}$, and the latter being a pure lattice symmetry, i.e., $\{E\|M_{100}\}$, in SSG $221.1.6.1.P$.

In Fig. 4(c), we show the structure of Mn_3Y ($Y =$ Ga, Ge, and Sn), which has a hexagonal lattice with Mn atoms forming two kagome sublayers stacked along the c axis. The magnetic moments of Mn atoms are oriented in the $(1, 1, 0)$, $(-1, 0, 0)$, and $(0, -1, 0)$ directions, respectively, written under a_1, a_2, a_3 axes. The SG of this structure is SG 194 $P6_3/mmc$, and the pure lattice group is $P2_1/m$, generated by the inversion $\mathcal{P}$ and $\{M_z|(a_3/2)\}$. The quotient group is isomorphic to the previous example, i.e., C_{3v}, but has different operations, with generators $\{3_{001}^-\|3_{001}^+\}$ and $\{2_{010}\|M_{010}\}$ (or, equivalently, $\{M_{210}\|M_{010}\}$). It is worth mentioning that, for the former generator, its real-space operation is a $\frac{2}{3}\pi$ rotation while the spin operation is a $-\frac{2}{3}\pi$ rotation, which is not allowed in MSG. The SSG is then identified as $194.1.6.1.P$ in our database, with a coplanar spin-only group given in Eq. (13). The MSG of this material is $63.463\ Cmc'm'$, generated by $\{E\|\mathcal{P}\}$, $\{2_{010}\|M_{010}\}$, and $\{2_{001}\|M_{001}|(a_3/2)\}\cdot\mathcal{T} \sim \{M_{001}\|M_{001}|(a_3/2)\}$. This MSG can be seen a subgroup of SSG $194.1.6.1.P$ by breaking $\{3_{001}^-\|3_{001}^+\}$ and the coplanar spin-only group. Remark that there exist two entries of Mn_3Sn on the Bilbao crystallographic server [6,79], which come from the same Ref. [90] and differ by an overall C_{4z} spin rotation. These two magnetic structures share the same SSG but with different conventions of spin rotations.

At last, we introduce a noncoplanar magnetic structure of Mn_3Y ($Y =$ Ga, Ge, and Sn) depicted in Fig. 4(d), which can be obtained by imposing a hydrostatic pressure up to 5 GPa to the coplanar magnetic structure in Fig. 4(c) according to Ref. [91]. The magnetic moments of Mn atoms are along $(1, -1, m_z)$, $(1, 2, m_z)$, and $(-2, -1, m_z)$ directions. The specific value of the z component m_z ($\neq 0$) is inessential, as it does not affect the SSG. To demonstrate how to obtain the SSG of this novel magnetic structure, we divide the transition from coplanar to noncoplanar order into two stages. In the first stage, the coplanar magnetic moments in Fig. 4(c) are rotated by $\pi/2$ in the z direction in spin space, which leaves the SSG (i.e., $194.1.6.1.P$) unchanged, as the spin and real space are unlocked. We remark that in SSGs the axes of the spin space can be chosen arbitrarily, while in MSG they cannot. In the second stage, the magnetic moments obtain a z component of equal magnitude, leading to a noncoplanar order that breaks the coplanar spin-only group symmetries. The SSG is then identified as $194.1.6.1$, with generators of the quotient group being $\{3_{001}^+\|3_{001}^-\}$ and $\{M_{210}\|M_{010}\}$ (note that $\{2_{010}\|M_{010}\}$ is broken). This noncoplanar SSG has the

same number of operations as the coplanar SSG 194.1.6.1.P by breaking the coplanar spin-only group, while the spin rotations undergo a spin-space coordinate transformation of $\pi/2$ rotation in the z direction. The MSG of this noncoplanar structure is $12.62\,C2'/m'$, with generators being inversion and $\{M_{100}\|2_{100}\}$. It can be seen that this MSG contains a significantly smaller number of operations compared with the SSG 194.1.6.1.

We remark that, in these four examples, all SG operations (obtained by ignoring magnetic moments) are maintained in the SSGs by assigning proper spin rotations, and the first number in the label of the identified SSG (i.e., N_{SG} in $N_{SG}.I_k.I_t.N_{3Drep}$) is the same as the SG. However, this does not necessarily hold for all magnetic structures. For example, consider a material with randomly generated magnetic moments. Then, no proper spin rotation could be assigned to SG operations, and, thus, the SSG has only the identity operation.

VI. APPLICATIONS OF SSGS

In this section, we discuss potential applications of SSGs. It contains four main parts: (i) the representation theory in SSGs with band representations of Mn_3Sn as a concrete example; (ii) topological states protected by SSG symmetries; (iii) spin texture structures under SSGs; and (iv) refining neutron scattering patterns using SSG symmetries.

A. Representation theory in SSGs

The representation theory of SGs and MSGs has been pivotal in advancing the study of materials, including the topological quantum chemistry [18,39] and symmetry-based indicators [25,44,92] for diagnosing topological crystalline phases. The introduction of SSGs significantly expands the symmetry landscape, potentially unveiling a richer array of physical phenomena in magnetic materials, particularly those characterized by weak SOC. In Ref. [47], the authors (including several authors of the current manuscript) study the corepresentation of noncoplanar SSGs with supercell k index $I_k = 2$, where the little cogroup is $P \times Z_2^T$, with P being one of 32 crystallographic point groups and $Z_2^T = \{E, \mathcal{T}\}$. A 12-fold fermion and 13 Dirac nodal line nexus are discovered which are topological band nodes that can be realized only in SSGs. In Ref. [93], the representation theory in SSG is studied using the complete sets of commuting operators.

In the following, we give a brief introduction to the representation theory in SSGs, with a more thorough investigation left to future work. We use Mn_3Sn as an example and compute the IRREPs for its electronic bands. We show the superiority of SSGs over MSGs by correctly capturing the multiple high-dimensional degeneracy in the band structure of Mn_3Sn.

1. Projective representations in SSGs

We first provide a brief introduction to the projective corepresentation theory in SSGs. We restrict ourselves to the spinful representations for electron systems for the little groups in the BZ. The spinless representations can also be constructed similarly.

To begin with, denote the representation of an SSG operation as $D(g)$ if g is unitary and $D(g)\kappa$ if antiunitary, where $D(g)$ is the representation matrix and κ the complex conjugation operator that satisfies $\kappa^2 = 1$ and $\kappa u = u^*\kappa$ for any matrix u. Define the multiplicity relationship of the representation matrices as

$$D(g_1)D(g_2)^{s(g_1)} = \omega(g_1, g_2)D(g_3), \qquad (33)$$

where $D(g_2)^{s(g_1)}$ indicates $D(g_2)$ when g_1 is unitary and $D(g_2)^*$ when g_1 is antiunitary. The factor $\omega(g_1, g_2)$ is a complex number with unit modulus, and the collection of $\omega(g_1 \in G, g_2 \in G)$ constitutes the factor system of the group, which should follow the equation

$$\omega(g_1, g_2)\omega(g_1g_2, g_3) = \omega(g_2, g_3)^{s(g_1)}\omega(g_1, g_2g_3). \quad (34)$$

We consider the factor system of an SSG at a high-symmetry point $\boldsymbol{k}$ in the BZ of an SSG, which is constructed by two parts: the SU(2) factor from spin rotations and the non-symmorphic translation factor. The SU(2) factor ω_1 originates from the two-to-one homomorphic relationship between SU(2) and SO(3) matrices and can take only the values of 1 or -1. The nonsymmorphic translation factor ω_2, however, is nontrivial only at the non-Γ momentum of the BZ in nonsymmorphic SSGs. For two group elements $g_1 = \{U_1\|R_1|\boldsymbol{\tau}_1\}$ and $g_2 = \{U_2\|R_2|\boldsymbol{\tau}_2\}$, their translation factor is chosen as

$$\omega_2(g_1, g_2) = e^{-i\boldsymbol{K}_1 \cdot \boldsymbol{\tau}_2}, \qquad \boldsymbol{K}_1 = s(g_1)(g_1^{-1}\boldsymbol{k} - \boldsymbol{k}), \qquad (35)$$

where $s(g_1) = 1$ or -1 when g_1 is unitary or antiunitary, respectively. It can be proven that the factor system, composed of these two parts, satisfies the combination relations required for projective representations. In the representation theory of SSGs, fixing the choice of this factor system can avoid the arbitrariness of the overall phase in the representation.

Based on the method, we construct the factor system for the little group of SSG at all high-symmetry points. The factor system is crucial for the representation of groups. We remark that, although an SSG is isomorphic to an MSG [94] when governed by the same multiplication relations and antiunitary parts, they do not share the same factor system. Thus, the IRREPs in SSGs are, in general, different from those in MSGs. This subtlety can be exemplified by the difference between the single- and double-group representations of an SG, where the double group has nontrivial spin factor systems.

With the multiplication relations and factor systems of SSGs derived, the IRREPs can then be constructed. In particular, we first consider the regular antiunitary projective corepresentations. Regular representations are, in general, reducible. It can be proven that such regular representations always encompass all IRREPs. Moreover, there are mathematical methods for reducing group representations, including the use of complete sets of commuting operators [93,95] and Hamiltonian methods [96]. By following the Hamiltonian method, we construct all the irreducible representations of the little groups at all high-symmetry points for SSGs, which we leave to future work.

2. Band structure and IRREPs of Mn_3Sn

We use Mn_3Sn as an example to show the application of IRREPs of SSGs in the electronic band structures. We consider the coplanar-ordered Mn_3Sn. Its band structure with and without SOC is shown in Fig. 5(a). SOC has only minor effects on the bands of Mn_3Sn, confirming its weak SOC nature and justifying the usage of SSGs.

In Fig. 5(b), we show the enlarged bands near E_f along $\Gamma - A - L$. We first use MSG to compute the IRREPs. The coplanar-ordered Mn_3Sn has MSG 63.463$Cmc'm'$, which is generated by $\{E\|\mathcal{P}\}$, $\{2_{010}\|M_{010}\}$, and $\{2_{001}\|M_{001}|(c/2)\} \cdot \mathcal{T}$. At Γ, MSG 63.463 has only 1D (double) IRREPs, which cannot explain the 2D degeneracies at Γ. We use SYMTOPO [97] to identify the characters of unitary operations of these bands, with results summarized in Supplemental Material Sec. VIII [81].

Next, we consider SSG 194.1.6.1.P of coplanar Mn_3Sn. This SSG has a unitary generator $\{3_{001}^-\|3_{001}^+\}$ and a pure lattice operation $\{E\|2_{001}|(z/2)\}$ besides the three generators in MSG $Cmc'm'$. Utilizing the method described in the previous section for constructing antiunitary projective
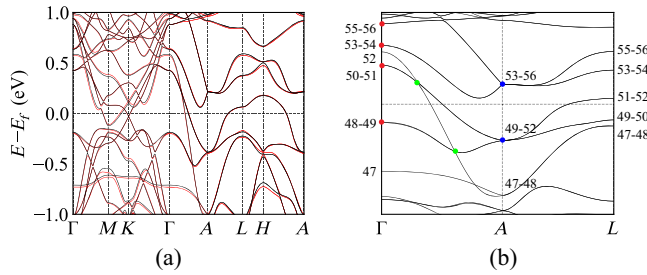
representations, we obtain all the irreducible representations of this group. At the Γ point, 194.1.6.1.P has 12 inequivalent IRREPs, including eight one-dimensional and four two-dimensional IRREPs. The character table is presented in Supplemental Material Sec. VIII [81]. With the character table of the SSG, we can successfully label each group of bands using the group's irreducible representations as shown in Table V. We add an "S" prefix to the labels of these IRREPs to distinguish them from the IRREPs of the MSG.

At the boundaries of BZ, nonsymmorphic operations could lead to higher degeneracies. As can be seen in Fig. 5(b), the bands at the A point exhibit both twofold and fourfold degeneracies. The MSG $Cmc'm'$ has only IRREPs of up to 2D at A, thus failing to explain the 4D degeneracy. This necessitates the introduction of SSG. Compared with the little group at Γ, the little group at A has the same group elements but possesses inequivalent factor systems. The character table of IRREP at A is listed in Table VI, showing the existence of one 2D and two 4D IRREPs. This gives a satisfying match to the density-functional theory band structure. Along the $A - L$ path, the SSG has only 2D irreducible representations, which is also consistent with the behavior of the bands along this path in Fig. 5(b).

Moreover, along the $\Gamma - A$ path, two threefold degeneracies are observed, protected by the symmetries of the SSG. While the MSG has only 1D representations along this path, SSG has four 1D and two 2D representations. Therefore, these two threefold degeneracies, resulting from

TABLE V. The band representations of Mn_3Sn at Γ using IRREPs of SSG 194.1.6.1.P. Operators $g_1 = \{E\|\mathcal{P}\}$, $g_2 = \{2_{010}\|M_{010}\}$, $g_3 = \{3_{001}^-\|3_{001}^+\}$, and $g_4 = \{E\|2_{001}|\frac{z}{2}\}$ are generators of SSG. The 2D degenerate points cannot be captured by IRREPs of the MSG.

Bands	E	g_1	g_2	g_3	g_4	IRREPs
47	1	1	i	-1	-1	$^S\bar{\Gamma}_3$
$48 + 49$	2	-2	0	1	2	$^S\bar{\Gamma}_{11}$
$50 + 51$	2	2	0	1	-2	$^S\bar{\Gamma}_{10}$
52	1	-1	i	-1	1	$^S\bar{\Gamma}_6$
$53 + 54$	2	-2	0	1	2	$^S\bar{\Gamma}_{11}$
$55 + 56$	2	2	0	1	2	$^S\bar{\Gamma}_{12}$

FIG. 5. Band structure and degeneracy of Mn_3Sn. (a) Band structure of Mn_3Sn near the Fermi level E_f, where the red lines represent the bands with SOC and the black lines represent the bands without SOC. SOC has only minor effects on the band structure of Mn_3Sn. (b) Enlarged band structure near E_f of Mn_3Sn along the $\Gamma - A - L$ path for bands 47–56. Twofold degeneracies (red dots) at Γ and fourfold degeneracies (blue dots) at A are observed. There are also 3D crossing points (green dots) along the $\Gamma - A$ path. These high-dimensional degenerate points can be captured only by the representation theory of SSGs (see Tables V and VI) but cannot by MSG.

TABLE VI. Character table of SSG 194.1.6.1.P at the A point. In the band structure of Mn_3Sn shown in Fig. 5(b), bands 47 and 48 have 2D $^S\bar{A}_1$ IRREP, while bands 49–52 and 53–56 share 4D $^S\bar{A}_3$ IRREP.

IRREPs	E	$\{E\|\mathcal{P}\}$	$\{2_{010}\|M_{010}\}$	$\{3_{001}^-\|3_{001}^+\}$	$\{E\|2_{001}|\frac{z}{2}\}$
$^S\bar{A}_1$	2	0	2i	-2	0
$^S\bar{A}_2$	2	0	-2i	-2	0
$^S\bar{A}_3$	4	0	0	2	0

the crossing of doubly degenerate bands with nondegenerate bands, are uniquely captured by the SSG.

We remark that the MSG of a specific material is always a subgroup of its SSG; thus, the IRREPs of the SSG can be decomposed into IRREPs of the MSG, either reducible or irreducible. For instance, the $^S\bar{\Gamma}_{11}$ IRREP in the SSG is reduced to $\bar{\Gamma}_5, \bar{\Gamma}_6$ in the MSG. With the IRREPs of MSG, the 2D, 3D, and 4D degeneracies in Mn_3Sn can be explained only as accidental (except for the 2D IRREPs at A). Only with SSG can we faithfully identify the high-dimensional degeneracies in the band structures of magnetic materials with weak SOC.

B. Example of topological states protected by SSG

In this section, we propose two new gapped topological states protected by SSG symmetries. We explicitly construct the IRREPs in these two SSGs and identify the topological surface states protected by the bulk topological states. We show that the nontrivial spin rotations in SSGs have important consequences in the IRREPs and topology.

Before starting, we discuss briefly some key aspects of the *real-space recipe* [25,26,44,98] in SSGs, which could be used to construct the complete topological classifications. The real-space recipe converts the problem of topological classification (i.e., exhausting all inequivalent topological states for a given symmetry group) into a "LEGO" puzzle, where one uses lower-dimensional topological building blocks to construct (gapped) 3D topological states. The lower-dimensional building blocks have gapless edge states, which need to be combined properly so that the resultant 3D states are gapped (i.e., the no open-edge condition). The obtained 3D states are subject to the so-called "bubble equivalence," a process that removes equivalent states. A simplified case in the real-space recipe is the *layer construction* [25], where the 3D topological states are built from 2D infinitely large layers. Generic 3D topological states are formed by small pieces of finite lower-dimensional states.

We then discuss some unique properties of the real-space recipe in SSGs and compare those in MSGs. First, unlike MSGs where only 2D Chern or mirror Chern insulators can be used as the lower-dimensional building blocks, SSGs could also host 2D topological insulators [48,94] protected by effective TRS symmetry $\mathcal{T}_M = \{E\|M\|\mathbf{0}\} \cdot \mathcal{T}$, with $\mathcal{T}_M^2 = -1$, where M is a mirror reflection along a certain direction. Second, there exists effective TRS on 1D lines in SSG, which could protect helical edge modes. These effective TRS include $\mathcal{T}_M = \{E\|M\|\mathbf{0}\} \cdot \mathcal{T}$ and $\mathcal{T}_{C_2} = \{E\|C_2\|\mathbf{0}\} \cdot \mathcal{T}$, which all square to -1. Third, there exist two types of mirror symmetries in SSG, i.e., the pure mirror without spin rotation $\{E\|M\|\mathbf{0}\}$, which has eigenvalue ± 1, and the mirror with spin rotation $\{U_M\|M\|\mathbf{0}\}$ (where $U_M = M \cdot \mathcal{P}$ is a C_2 rotation), which has eigenvalue $\pm i$. We leave a complete real-space construction of topological states in SSGs for further work.

In the following, we consider two simple but novel examples of gapped topological states in SSGs. We start with a detailed discussion of the IRREPs of the SSG, which can be derived from the IRREPs of a corresponding MSG through a folding and shifting process of the BZ. The topological states in the SSG are then constructed using the real-space recipe.

1. SSG 1.4.1.2

We first consider SSG 1.4.1.2 with generator $g = \{C_4\|E\|0,0,\frac{1}{4}\} \cdot \mathcal{T}$, where the translation is written under magnetic unit cell bases [i.e., $(0, 0, 1)$ is a lattice translation]. We drive the (spinful) IRREPs in this SSG and then build a $\mathbb{Z}_2$ topological state protected by the anti-unitary operation g, similar to the antiferromagnetic topological insulator [99,100].

IRREPs.—Based on the algorithm introduced in Sec. VI A, we obtain the IRREPs at eight time-reversal-invariant momenta (TRIMs), with results summarizing in Table VII. There is only one 2D IRREP for TRIMs on the $k_z = 0$ plane, while one 1D and one 2D IRREP for TRIMs on the $k_z = \pi$ plane. These IRREPs can be understood from the IRREPs of MSG 1.3 P_S1 with generator $g_M = \{E\|E\|0,0,\frac{1}{2}\} \cdot \mathcal{T}$. The unit cell of SSG 1.4.1.2 can be seen as a doubled one of MSG 1.3. In MSG 1.3, there are 2D IRREPs (i.e., Kramers' pairs) on $k_z = 0$ TRIMs and 1D IRREPs on $k_z = \pi$ TRIMs. In the following, we show that the IRREPs of SSG 1.4.1.2 can be obtained from the IRREPs of MSG 1.3 through a folding process of the BZ, together with a subtle shifting of BZ in the k_z direction resulting from the nontrivial spin rotation.

Define $h = \{C_2\|E\|0,0,\frac{1}{2}\}$ which has a representation matrix satisfying $D(h) = -D(g^2)$, where the minus sign comes from $\mathcal{T}^2 = -1$. This unitary operation h can serve as a new translation group generator, as h commutes with g and all other translations. Denote the BZ defined from h as mBZ. In the mBZ, the TRIMs on the $k_z = 0$ plane have $D(g^2) = -1$ which give a Kramers' pair, while on the $k_z = \pi$ plane $D(g^2) = +1$ and gives only 1D IRREPs. This is the same result as in MSG 1.3.

TABLE VII. The summary of IRREPs at TRIMs in SSG 1.4.1.2 and SSG 1.4.1.3. In the table, "Dirac point" means the 2D IRREP forms a Dirac crossing point, while "nodal line" means the 2D IRREP is part of a nodal line in the BZ. In SSG 1.4.1.3, the k_z is omitted in the coordinate of TRIMs.

SSG 1.4.1.2	$k_z = 0$ TRIMs	$k_z = \pi$ TRIMs	
IRREP	One 2D (Nodal line)	One 1D, One 2D (Dirac point)	
SSG 1.4.1.3	(0,0)	(π,π)	$(0,\pi),(\pi,0)$
IRREP	Two 1D	Two 2D (Dirac point)	One 2D (Nodal line)

Then, we turn to the real BZ of the SSG defined by $\{E\|E|0,0,1\}$. The SSG BZ is the folded version of the mBZ. Notice that $D(h^2) = -D(\{E\|E|0,0,1\})$, where the minus sign comes from the spin rotation as $U_{C_2}^2 = -1$ [U_R denotes the corresponding SU(2) spin rotation of R]. We consider TRIMs on $k_z = 0$ and π planes separately.

(i) For TRIMs with $k_z = \pi$, we have $D(h^2) = +1$, as $e^{ik_z} = -1$ when $k_z = \pi$. In the mBZ, all the TRIMs on $k_z = 0, \pi$ planes satisfy $D(h^2) = +1$ and are mapped to the $k_z = \pi$ TRIMs in the SSG BZ. Thus, the 1D and 2D IRREPs coexist for the $k_z = \pi$ TRIMs. They are characterized by $D(h) = +1$ (for 2D IRREP) and $D(h) = -1$ (for 1D IRREP), respectively. The eigenvalue of h separates the states on the $k_z = \pi$ plane into two independent sectors. The 2D IRREP sector could protect $\mathbb{Z}_2$ topological flow [101,102] and give rise to the surface Dirac cone, while the 1D IRREP sector is an "audience" that does not hybridize with the states having the 2D IRREP.

(ii) For TRIMs with $k_z = 0$, we have $D(h^2) = -1$ and, thus, $D(h) = \pm i$. This corresponds to the $k_z = \pm(\pi/2)$ planes in the mBZ, which host only 1D IRREPs. After folding into the SSG BZ, 2D IRREPs are formed at TRIMs with $k_z = 0$, as $k_z = \pm(\pi/2)$ planes are related by g. Moreover, these 2D IRREPs on the $k_z = 0$ TRIMs in the SSG BZ must be part of a nodal line, as a result of folding from mBZ.

The Dirac cone and nodal lines in the SSG BZ can also be verified from the $\boldsymbol{k} \cdot \boldsymbol{p}$ theory. For the 2D IRREPs on TRIMs with $k_z = 0$ (denote as $D_{k_z=0}^{2D}$) and $k_z = \pi$ (denote as $D_{k_z=0}^{2D}$), their representation matrix can be chosen as

$$D_{k_z=0}^{2D}(g) = \begin{pmatrix} 0 & 1 \\ -i & 0 \end{pmatrix}, \quad D_{k_z=\pi}^{2D}(g) = \begin{pmatrix} 0 & 1 \\ -1 & 0 \end{pmatrix}. \quad (36)$$

The $\boldsymbol{k} \cdot \boldsymbol{p}$ effective Hamiltonians constructed from these representation have the following form.

(i) For a TRIM on the $k_z = 0$ plane, the $\boldsymbol{k} \cdot \boldsymbol{p}$ Hamiltonian has the form $(a_1\delta k_1 + a_2\delta k_2 + a_3\delta k_3)\sigma_z$, where $\delta\boldsymbol{k} = \boldsymbol{k} - \boldsymbol{k}_0$ is the deviation from TRIM $\boldsymbol{k}_0$ and $a_{i=1,2,3}$ are free parameters. A nodal line is given by $a_1\delta k_1 + a_2\delta k_2 + a_3\delta k_3 = 0$ that passes the TRIM.

(ii) For a TRIM on the $k_z = \pi$ plane, the $\boldsymbol{k} \cdot \boldsymbol{p}$ Hamiltonian has nine independent terms, i.e., all combinations between $\delta k_{i=1,2,3}$ and $\sigma_{i=x,y,z}$. Thus, linear Dirac crossings are allowed.

We also briefly mention the IRREPs in spinless systems, e.g., magnon bands. For spinless IRREPs in the mBZ, 2D Kramers pairs appear on the $k_z = \pi$ TRIMs, as $\mathcal{T}^2 = +1$. Then, $h^2 = \{E\|E|0,0,1\}$ in the SSG BZ. Thus, on the $k_z = 0$ TRIMs, there are both 2D Kramers' pairs and 1D IRREPs, while on the $k_z = \pi$ TRIMs there are 2D IRREPs

from folding $k_z = \pm(\pi/2)$ in the mBZ. It can be seen that the IRREPs on $k_z = 0$ and π planes are reversed for spinless and spinful systems.

Topological states.—This SSG protects a layer construction (LC) with a $\mathbb{Z}_2$ classification, as shown in Fig. 6(a). This LC (denoted as LC_S) consists of Chern layers with Chern number $C = 1$ on $z = (2n/4)$ planes and Chern layers with $C = -1$ on $z = (2n + 1/4), n \in \mathbb{Z}$ planes. Adjacent layers are related by g and, thus, have opposite Chern number. This state is topological, because the Chern layers can be deformed but cannot be eliminated as long as g is maintained. Its doubled state, however, can be trivialized, as Chern layers with $C = \pm1$ can then be moved together and canceled, leading to the $\mathbb{Z}_2$ classification.

LC_S can be understood from the layer construction of MSG 1.3 P_S1 (denoted as LC_M) with generator $g_M = \{E\|E|0,0,\frac{1}{2}\} \cdot \mathcal{T}$. LC_M has two Chern layers with Chern number $C = \pm1$ on $z = 0, \frac{1}{2}$ planes in the unit cell. In MSG 1.3, TRIMs on the $k_z = 0$ plane host Kramers' pairs. For an open boundary along the z direction that preserves g_M, a single Dirac (or, more generally, an odd number) cone will appear on TRIMs with $k_z = 0$ in the surface BZ, which can be verified from the 2D IRREPs on $k_z = 0$ TRIMs. LC_S can be seen as the doubled LC_M along the z direction. As LC_M holds a single Dirac cone in the surface BZ, LS_S also hosts a single Dirac cone. Doubling of the unit cell leads to the folding of the BZ in LC_M, which maintains the number of surface Dirac cones.

Remark that similar topological states also exist in SSGs generated by $\{C_{2n}\|E|0,0,(1/2n)\} \cdot \mathcal{T}, n \in \mathbb{Z}, n \geq 1$, which host a single surface Dirac cone.

2. SSG 1.4.1.3

In the second example, we consider SSG 1.4.1.3, with two antiunitary operations

$$g_x\mathcal{T} = \left\{C_{2x}\|E|\frac{1}{2},0,0\right\} \cdot \mathcal{T}, \quad g_y\mathcal{T} = \left\{C_{2y}\|E|0,\frac{1}{2},0\right\} \cdot \mathcal{T}. \quad (37)$$

This SSG also has unitary operations with nontrivial spin rotations: $s_1 = \{C_{2z}\|E|\frac{1}{2},\frac{1}{2},0\}$ and $s_2 = \{C_{2z}\|E|-\frac{1}{2},\frac{1}{2},0\}$.

IRREPs.—We start from the IRREPs in SSG 1.4.1.3, with results summarizing in Table VII. The unit cell basis in the xy plane of SSG 1.4.1.3 can be taken as $A_1 = (1,0)$, $A_2 = (0,1)$. Denote the corresponding momentum in the SSG BZ as (k_1, k_2). We have omitted the z direction for simplicity. In SSG 1.4.1.3, the representation of operations satisfies

$$D[(g_x\mathcal{T})^2] = D(\{E\|E|1,0,0\}) = D(s_1)D(s_2^{-1}),$$
$$D[(g_y\mathcal{T})^2] = D(\{E\|E|0,1,0\}) = -D(s_1)D(s_2), \quad (38)$$

$$D(s_1^2) = -D(\{E\|E|1,1,0\}),$$
$$D(s_2^2) = -D(\{E\|E|-1,1,0\}), \qquad (39)$$

where the minus sign comes from the spin rotation as $U_{C_{2z}}^2 = -1$. Similar to the previous SSG 1.4.1.2, we take s_1 and s_2 as the translation group generators and denote the BZ thus defined as mBZ. The IRREPs of this SSG can also be built from the mBZ through a folding and shifting process. A subtle difference here is these two operations do not commute with $g_{x,y}\mathcal{T}$ and will modify the coordinates of TRIMs and their IRREPs in the mBZ, which we show in the following.

We first identify the TRIMs in the mBZ. By definition, TRIMs are the momenta that are invariant under the antiunitary operation (but not necessarily always have coordinate $k_i = 0, \pi$). As

$$D(g_x\mathcal{T})D(s_{i=1,2})D(g_x\mathcal{T})^{-1} = -D^*(s_{i=1,2}), \quad (40)$$

where the minus sign comes from the spin rotations, TRIMs must have $D(s_{1,2}) = e^{ik_m \cdot s_i} = \pm i$ (note here s_i are treated as the translation group generators, and k_m is defined in the mBZ). Thus, TRIMs have coordinate $k_m = [\pm(\pi/2), \pm(\pi/2)]$ in the mBZ. We then identify which TRIMs host Kramers' degeneracy by requiring $D[(g_{x,y}\mathcal{T})^2] = -1$. Direct computation shows the TRIMs at $\pm[(\pi/2), -(\pi/2)]$ satisfy. The other two TRIMs have $D[(g_{x,y}\mathcal{T})^2] = +1$ and, thus, host only 1D IRREP.

With IRREPs at TRIMs in the mBZ, we then construct those in the SSG BZ. As shown in Eq. (38), we have

$$D(A_1) = D(s_1)D(s_2^{-1}), \quad D(A_2) = -D(s_1)D(s_2). \quad (41)$$

This relation is used to map the TRIMs between SSG BZ and the mBZ.

(i) For the (0,0) TRIM, there are two 1D IRREPs. This is because, at this TRIM, $D(A_1) = D(A_2) = e^{ik_s \cdot A_i} = +1$ (k_s is defined in the SSG BZ). Thus, it can be mapped from the $\pm[(\pi/2), (\pi/2)]$ TRIMs in the mBZ, as $D(A_1) = D(s_1)D(s_2^{-1}) = e^{ik_m \cdot s_1}e^{-ik_m \cdot s_2} = 1$ when $k_m = \pm[(\pi/2), (\pi/2)]$ [$D(A_2)$ is similar]. Since these two TRIMs in the mBZ each host one 1D IRREP, they give two 1D IRREPs at (0,0) in the SSG BZ.

(ii) For the (π, π) TRIM, there are two 2D IRREPs that protect Dirac crossings, because at this TRIM, $D(A_1) = D(A_2) = -1$ and can be mapped from the $\pm[(\pi/2), -(\pi/2)]$ TRIMs in the mBZ, which host 2D Kramers' pairs.

(iii) For the $(0, \pi)$ TRIMs, there is one 2D IRREP coming from folding. This is because at this TRIM $D(A_1) = +1$, $D(A_2) = -1$ and can be mapped from the $(0, 0), (\pi, \pi)$ in the mBZ. In the mBZ,
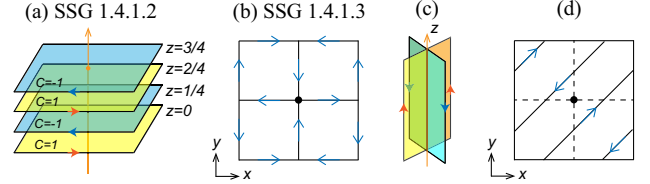

FIG. 6. (a) A layer construction protected by SSG 1.4.1.2. (b),(c) A nonlayer construction protected by SSG 1.4.1.3. (b) is from the top view, where arrows denote the direction of chiral edge modes when the boundary is open. (c) is from the side view, in which we show only the four Chern patches inside a unit cell and omit the patches on the boundary. (d) The layer construction deformed from the nonlayer construction in (b), which has four Chern layers in a unit cell with alternating Chern numbers.

$(0,0), (\pi, \pi)$ are generic points with only 1D trivial IRREP and are related by $g_{x,y}\mathcal{T}$. The 2D IRREP at $(0, \pi)$ in the SSG BZ cannot support Dirac crossings but must be part of a nodal line due to the folding of BZ.

(iv) The $(\pi, 0)$ TRIM is similar to $(0, \pi)$, which host one 2D IRREP from folding the 1D IRREPs at the $(0, \pi), (\pi, 0)$ in the mBZ.

Topological states.—SSG 1.4.1.3 protects a $\mathbb{Z}_2$ nonlayer construction, as shown in Figs. 6(b) and 6(c). This nonlayer construction is an axion insulator with a vanishing net Chern number, protected by the antiunitary SSG translations $g_{x,y}\mathcal{T}$. It can be deformed into a layer construction as shown in Fig. 6(d). This state is topological, because the Chern layers can be deformed but cannot be removed when $g_{x,y}\mathcal{T}$ is maintained. Two copies of the states are topologically trivial as the Chern layers can then be eliminated, validating the $\mathbb{Z}_2$ classification.

We then consider the surface states of this topological state. Surface Dirac cones could appear on only surface BZ that supports the partner-switching $\mathbb{Z}_2$ topological flow of the surface Dirac cone [101,102], which normally requires an even number of TRIMs that can host a Kramers' pair. From the IRREPs, the xz or yz surface hosts two TRIMs with Kramers' pairs and, thus, can host a single (or odd number of) surface Dirac cone. The xy surface has only one TRIM at (π, π) that hosts a Kramers' pair. Surprisingly, this surface can still protect the topological surface Dirac cone, as the mBZ has two TRIMs with a Kramers' pair on this surface and supports the $\mathbb{Z}_2$ flow. The folding process will not change the topological nature of the flow. In the SSG BZ, the topological $\mathbb{Z}_2$ flow starts from a Dirac cone at (π, π) and connects to the nodal line [which passes $(\pi, 0)$ and $(0, \pi)$] and then goes bask to (π, π). This surface state is unique in SSG, resulting from the modified group structure given by the spin rotations.

C. Spin textures

The spin texture $S(k)$ is defined as the expectation value of the spin operator on a Bloch state [94], i.e.,

$S(k) = \langle \psi_k | \sigma | \psi_k \rangle$, which is usually defined on the Fermi surface. Reference [94] gives a detailed discussion on the properties of the spin textures based on the SSG BZ. Motivated by Ref. [94], we give a brief discussion on the symmetry properties of the spin textures in SSGs, focusing on the dimension of the spin texture constraint by the SSG operations.

For an SSG operation $g = \{U_R \| R | \tau\}$, the spin texture $S(k)$ transforms as

$$g S(k) = U_R S(s_g R^{-1} k), \qquad (42)$$

where $s_g = \pm 1$ for $\det(U_R) = \pm 1$; i.e., when $\det(U_R) = -1$, g is antiunitary and reverse k. We first consider the effects of spin-only group S_0 on $S(k)$.

(i) For collinear SSGs, the spin rotation $\{C_\theta \| E | 0\} \in S_0$ enforces $S(k) = [0, 0, S_z(k)]$ to be collinear. When the SSG also has $\mathcal{PT}$ or antiunitary translation $\mathcal{T} \cdot \tau$, spin degeneracy is guaranteed over the whole BZ, which will enforce $S(k) = 0$. Without these two types of symmetries, spin splitting is expected and the magnetic order is described as altermagnetism [51–53] recently, which allows for nontrivial spin texture.

(ii) For coplanar SSGs, $\{M_z \| E | 0\} \sim \{C_{2z} \| E | 0\} \cdot \mathcal{T} \in S_0$ enforces $S(k) = M_z S(-k)$, and $S(k)$ vanishes on TRIMs.

(iii) For the nonmagnetic case, $S_0 = O(3)$ will enforce $S(k) = 0$. Remark that, in the presence of SOC, the O(3) spin-only group is broken and the spin texture is, in general, nonvanishing.

We then consider general SSGs. The following SSG operations will reduce the dimension of $S(k)$.

(i) When the SSG contains $\{P \| P | 0\} \sim \mathcal{PT}$, $S(k)$ is enforced to be zero.

(ii) When the SSG contains $\{C_n \| E | \tau\}$, we have $S(k) = C_n S(k)$ and, thus, $S(k)$ must be collinear along the C_n direction.

(iii) When the SSG contains $\{M \| P | 0\}$ where M is a mirror, we have $S(k) = M S(k)$ and, thus, $S(k)$ must be coplanar on the mirror plane.

We then argue that the noncrystallographic spin rotations in SSGs will enforce $S(k)$ to be collinear to vanishing. For SSGs with noncrystallographic spin rotations, there always exist spin rotations C_p ($p \neq 2, 3, 4, 6$). We argue that, in such SSG S, there exists at least one operation with the form $g = \{C_n \| E | \tau\}$, i.e., a noncrystallographic spin rotation accompanied by a pure translation. This operation enforces the collinear spin texture as discussed in the previous paragraph. We then prove the existence of g. Suppose the noncrystallographic C_p spin rotation in S has some real-space rotation R and translation τ part, i.e., $h = \{C_p \| R | \tau\}$. As R can be only crystallographic with rank $m = 1, 2, 3, 4, 6$, we have $h^m = \{C_p^m \| E | \tau'\}$. This operation has the same form as g, i.e., a noncrystallographic spin

rotation C_p^m with no real-space rotation but only a translation. The translation part must be nonzero, because, otherwise, h^m belongs to the spin-only group S_0, which contradicts the assumption that the spin-only group and the spin-only-free group have only a trivial intersection.

D. Refine magnetic neutron diffraction patterns with SSG

In this section, we consider the application of SSGs to facilitate the refinement of magnetic orderings from magnetic neutron diffraction. We first review the refinement algorithm based on MSGs in the literature [103,104] and then extend it to SSGs. We use Mn_3Sn as a realistic example to demonstrate the advantage of SSG in the refinement by reducing the number of refining parameters.

1. Algorithm of refinement

In the literature, a commonly used software for refining neutron diffraction is FULLPROF [103], which has a representational analysis module "simulated annealing and representational analysis" (SARAh) [104]. SARAh could list all possible MSGs and corresponding magnetic structures for a given nonmagnetic SG and propagation vector. Our algorithm based on SSG has the same spirit and could be integrated into their work flow by extending MSGs to SSGs.

We start with the necessary experimental information that can be measured before refining magnetic structures: (i) The nonmagnetic SG $\mathcal{G}$ of the material refined based on x-ray diffraction measurements in the magnetic phase or neutron diffraction measurement in the paramagnetic phase if assuming there is no atomic displacement during the magnetic transition. $\mathcal{G}$ gives the symmetries of the crystal structure by ignoring the magnetic moments. (ii) The magnetic unit cell (propagation vector) obtained from new Bragg peaks shown in neutron diffraction patterns compared with the paramagnetic pattern, which could be either the same as the nonmagnetic unit cell (propagation vector $q = 0$) or an enlarged supercell (propagation vector $q \neq 0$). (iii) The neutron diffraction patterns used for fitting in the refinement. (iv) The net magnetic moment and its direction. Zero net magnetic moment indicates the AFM order. One can also distinguish collinear (together with the direction of moments), coplanar noncollinear (together with the plane of moments), and noncoplanar magnetic configurations by, for example, measuring anisotropic magnetization, e.g., magnetic susceptibility measurements on single crystals.

With the aforementioned experimental data, the following algorithm can be adopted for refinement based on MSG [103,104].

(1) List all MSGs $\mathcal{M}$ that are compatible with the nonmagnetic SG $\mathcal{G}$ and magnetic unit cell (propagation vector). In the case of multiple propagation vectors, the magnetic unit cell can also be constructed, where

different combination coefficients of propagation vectors give different symmetry groups.

(2) For each $\mathcal{M}$, find the Wyckoff positions of the magnetic atoms and the symmetry-allowed components of magnetic moments. The moment could be (i) free (noncoplanar), parametrized by (m_x, m_y, m_z); (ii) restricted on a certain plane (coplanar noncollinear), for example, on $(m_x, m_y, 0)$; or (iii) restricted along a certain direction (collinear), for example, along $(0, 0, m_z)$. This step can also be done mathematically by decomposing the representations of the little group G_q operations on the magnetic moments into IRREPs of G_q, and the bases of these IRREPs give symmetry-independent magnetic moments [103].

(3) Parametrize the magnetic configuration using the symmetry-independent magnetic atoms. Assume there are N such atoms. Then, the number of fitting parameters is between N and $3N$. Fit the parameters to the neutron data and find the magnetic configuration with minimal error.

(4) If the fitting errors are large, the previous steps are repeated by considering the subgroups of $\mathcal{G}$ and their corresponding MSGs, as magnetic order could break the symmetry. Especially when the propagation vector already breaks some symmetries in $\mathcal{G}$, we could start from the corresponding subgroup at the beginning.

The refinement algorithm based on MSGs can be extended to SSGs straightforwardly. SSGs have the advantage of richer symmetry operations compared with MSGs and, thus, could reduce the number of fitting parameters.

To facilitate the usage of SSGs in the refinement, we also give an algorithm to determine the symmetry-allowed directions of magnetic moments for a given SSG. Consider an SSG $\mathcal{S}$ and a Wyckoff position with representative point s_0. The algorithm has the following steps.

(1) First, determine the site symmetry group G_{s_0} of s_0, which is formed by SSG operations that keep s_0 invariant, i.e., $G_{s_0} = \{g = \{U\|R|\tau\} \in \mathcal{S} | gs_0 = s_0 + \boldsymbol{R}\}$, where $\boldsymbol{R}$ is a lattice translation. Denote the spin-only site group as $G_{s_0}^0 = \{U\}$, where U is the spin rotations from all operations in Gs_0.

(2) We then consider the symmetry-allowed magnetic moments $\boldsymbol{M}_0$ at s_0, which should satisfy $U_i\boldsymbol{M}_0 = \boldsymbol{M}_0$, $\forall\ U_i \in G_{s_0}^0$. In practice, this equation can be transformed into finding the intersection of eigenspaces where all U_i have eigenvalues 1 or, more conveniently, finding the common null space of $\cup_i (U_i - \mathbf{1}_3)$. This eigenspace is classified into the following three scenarios.

   (a) If the dimension of the space is 0, then $\boldsymbol{M}_0 = \boldsymbol{0}$. This means, under SSG $\mathcal{S}$, the Wyckoff cannot host nonzero magnetic moments. In this case, when the magnetic atom is at this Wyckoff

position, SSG $\mathcal{S}$ should be excluded in the refinement.

   (b) If the dimension of the space is 1, then $\boldsymbol{M}_0$ is restricted to a specific direction. The magnitude of the magnetic moment is used as the sole refinement parameter.

   (c) If the dimension of the space is 2, then $\boldsymbol{M}_0$ is restricted to a plane and is parametrized by two parameters, i.e., the combination coefficients of two eigenvectors.

   (d) If the dimension of the space is 3, then $\boldsymbol{M}_0$ is free and has three parameters.

(3) Once $\boldsymbol{M}_0$ at s_0 is determined, we use other operations of the SSG to generate the magnetic moments at other sites s_i in this Wyckoff position.

With the algorithm above, we can parametrize the magnetic moments on Wyckoff positions for a given SSG $\mathcal{S}$. These parameters are used as input for the refinement of the neutron diffraction pattern.

We remark on one possible issue with SSGs—i.e., the spin space and real space are decoupled in SSGs, and, thus, the spin orientations could differ by an overall rotation without breaking any symmetry. This means the symmetry-independent moments are, in principle, all free under SSGs. This problem could be partly overcome as the direction of moments in collinear orders and the plane of moments in coplanar orders could be predetermined from experiments. We also remark that, in our database [75], the spin space has a fixed orientation; e.g., all collinear SSGs have the spin axis along the z direction in spin space. The convention may need to be tailored for realistic materials.

2. Example of Mn_3Sn

We take Mn_3Sn [90] as an example to exemplify the advantage of SSG in neutron diffraction refinement. As shown in Fig. 4(c), Mn_3Sn has nonmagnetic SG 194$P6_3/mmc$, with magnetic Mn atoms on the kagome 6h Wyckoff position and Sn atoms on the 2c position.

We start from a general consideration of how many SSGs could support nonzero magnetic moments on the 6h Wyckoff position from SG 194 without involving enlarged supercells, i.e., magnetic propagation vector $\boldsymbol{q} = (0, 0, 0)$. From our enumeration results, there are eight collinear, 40 (noncollinear) coplanar, and 152 noncoplanar SSGs constructed from SG 194 with $I_k = 1$. Despite the large number of SSGs, only two collinear, two coplanar, and four noncoplanar SSGs can support nonzero and inequivalent magnetic moments on the 6h position. The resultant magnetic structures from these eight SSGs are shown in Fig. 7, with the detailed directions of magnetic moments on each site of 6h tabulated in Table VIII. We discuss these SSGs in more detail.

  (i) For the collinear case, SSGs 194.1.1.1.L and 194.1.2.2.L both correspond to FM order in plane but FM and AFM out of plane, respectively. The

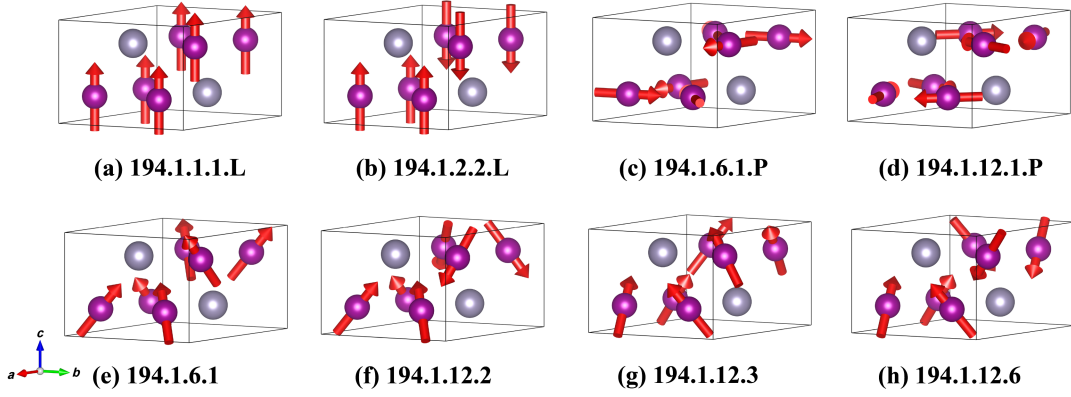FIG. 7. The of symmetry-allowed magnetic configurations on the 6h Wyckoff position in eight SSGs induced from SG 194 with $I_k = 1$. (a) and (b) are collinear orders. (c) and (d) are coplanar orders. (e)–(h) are noncoplanar orders. With SSGs, these magnetic configurations could be parametrized by only a few parameters.

magnetic configurations are parametrized by only one parameter m_z. Remark that 194.1.2.2.L has generator $\{M_z \| C_{2z} | a_3/2\} \sim \{C_{2z} \| C_{2z} | a_3/2\} \cdot \mathcal{T}$ that connects two Mn layers, which is altermagnetic with spin-split electronic bands.

(ii) For the coplanar case, SSG 194.1.6.1.P enforces the same magnetic moments on two Mn layers, while 194.1.12.1.P has opposite directional moments. These two magnetic configurations are also parametrized by only one parameter. The coplanar configuration described in Fig. 4(c) has SSG 194.1.6.1.P. We remark that, in Ref. [90], the authors did not consider the magnetic configuration given by 194.1.12.1.P, which has only a subtle difference compared with 194.1.6.1.P and might give a comparable error of refinement.

(iii) For the noncoplanar case, there are four SSGs: 194.1.6.1, 194.1.12.2, 194.1.12.3, and 194.1.12.6, each parametrized by two parameters. Among them, SSG 194.1.6.1 has two Mn layers sharing the same

direction of magnetic moments, which describes the experimental structure of Mn$_3$Sn reported in Ref. [91]. The other three possible noncoplanar SSGs give two inequivalent Mn layers.

Note that, among the large number of SSGs given by SG 194 with $I_k = 1$, many of them allow only magnetic moments with higher symmetries on Wyckoff position 6h and can be omitted. For example, some noncoplanar SSGs allow only collinear orders on 6h and, thus, are equivalent to a collinear SSG. Moreover, the directions of magnetic moments in each SSG tabulated in Supplemental Material Sec. IX [81] could change by an overall rotation, due to the decoupled nature of spin and real spaces in SSGs.

For comparison, we also consider magnetic moments restricted by the MSG of Mn$_3$Sn in coplanar and non-coplanar order, i.e., MSG 63.463$Cmc'm'$ and 12.62$C2'/m'$. For MSG 63.463, the 6h position splits into two symmetry-independent Wyckoff positions 8g and 4c, which gives four parameters. For MSG 12.62, 6h splits into 8j and 4i, which gives five parameters. These two MSGs have

TABLE VIII. SSGs from SG 194 with $I_k = 1$ and their symmetry-allowed magnetic moments on the 6h Wyckoff position of SG 194. There are two allowed collinear, two coplanar, and four noncoplanar SSGs. SSGs have the advantage of fewer free parameters in the magnetic moments compared with MSGs and could facilitate the refinement of magnetic structures from neutron diffraction patterns.

SSG number	$(-x, -2x, \frac{1}{4})$	$(2x, x, \frac{1}{4})$	$(-x, x, \frac{1}{4})$	$(x, 2x, \frac{3}{4})$	$(-2x, -x, \frac{3}{4})$	$(x, -x, \frac{3}{4})$
194.1.1.1.L	$(0, 0, m_z)$	$(0, 0, m_z)$	$(0, 0, m_z)$	$(0, 0, m_z)$	$(0, 0, m_z)$	$(0, 0, m_z)$
194.1.2.2.L	$(0, 0, m_z)$	$(0, 0, m_z)$	$(0, 0, m_z)$	$(0, 0, -m_z)$	$(0, 0, -m_z)$	$(0, 0, -m_z)$
194.1.6.1.P	$(-\frac{m_x}{2}, \frac{\sqrt{3}m_x}{2}, 0)$	$(-\frac{m_x}{2}, \frac{-\sqrt{3}m_x}{2}, 0)$	$(m_x, 0, 0)$	$(-\frac{m_x}{2}, \frac{\sqrt{3}m_x}{2}, 0)$	$(-\frac{m_x}{2}, -\frac{\sqrt{3}m_x}{2}, 0)$	$(m_x, 0, 0)$
194.1.12.1.P	$(-\frac{\sqrt{3}m_y}{2}, -\frac{m_y}{2}, 0)$	$(\frac{\sqrt{3}m_y}{2}, -\frac{m_y}{2}, 0)$	$(0, m_y, 0)$	$(\frac{\sqrt{3}m_y}{2}, \frac{m_y}{2}, 0)$	$(-\frac{\sqrt{3}m_y}{2}, \frac{m_y}{2}, 0)$	$(0, -m_y, 0)$
194.1.6.1	$(-\frac{m_x}{2}, \frac{\sqrt{3}m_x}{2}, m_z)$	$(-\frac{m_x}{2}, \frac{-\sqrt{3}m_x}{2}, m_z)$	$(m_x, 0, m_z)$	$(-\frac{m_x}{2}, \frac{\sqrt{3}m_x}{2}, m_z)$	$(-\frac{m_x}{2}, -\frac{\sqrt{3}m_x}{2}, m_z)$	$(m_x, 0, m_z)$
194.1.12.2	$(-\frac{m_x}{2}, \frac{\sqrt{3}m_x}{2}, m_z)$	$(-\frac{m_x}{2}, \frac{-\sqrt{3}m_x}{2}, m_z)$	$(m_x, 0, m_z)$	$(-\frac{m_x}{2}, \frac{\sqrt{3}m_x}{2}, -m_z)$	$(-\frac{m_x}{2}, -\frac{\sqrt{3}m_x}{2}, -m_z)$	$(m_x, 0, -m_z)$
194.1.12.3	$(-\frac{\sqrt{3}m_y}{2}, -\frac{m_y}{2}, m_z)$	$(\frac{\sqrt{3}m_y}{2}, -\frac{m_y}{2}, m_z)$	$(0, m_y, m_z)$	$(\frac{\sqrt{3}m_y}{2}, \frac{m_y}{2}, m_z)$	$(-\frac{\sqrt{3}m_y}{2}, \frac{m_y}{2}, m_z)$	$(0, -m_y, m_z)$
194.1.12.6	$(-\frac{\sqrt{3}m_y}{2}, -\frac{m_y}{2}, m_z)$	$(\frac{\sqrt{3}m_y}{2}, -\frac{m_y}{2}, m_z)$	$(0, m_y, m_z)$	$(\frac{\sqrt{3}m_y}{2}, \frac{m_y}{2}, -m_z)$	$(-\frac{\sqrt{3}m_y}{2}, \frac{m_y}{2}, -m_z)$	$(0, -m_y, -m_z)$

much lower symmetry compared with the SSGs in the same table, and the 6*h* Wyckoff position splits into multiple symmetry-independent Wyckoff positions. Thus, the independent components of the magnetic moments are increased and detrimental for the neutron refinements.

VII. CONCLUSIONS

In this work, we give an invariant subgroup-based algorithm to enumerate SSGs systematically. We implement the algorithm and find a vast number of SSGs. With the enumerated SSGs, the representation theory [96,105], new types of magnetic topological states, and novel quasiparticles protected by SSG symmetries can be readily explored in the future.

In addition to the applications of SSGs discussed in our work, it is noteworthy that SSGs offer valuable insights into the transport properties of magnetic materials with weak SOC. The enhanced symmetry framework provided by SSGs is instrumental in categorizing potential responses to various external fields. For instance, SSGs offer a deeper understanding of the anomalous Hall effect (AHE) in different magnetic materials. Collinear and coplanar magnetic materials have pure-spin operations that can be seen as effective time-reversal symmetry, which enforces the AHE to be zero when SOC is negligible [106,107]. With the inclusion of SOC, the degenerate points protected by SSG symmetries are lifted and could lead to large AHE. For noncoplanar magnetic materials, AHE could exist even without SOC [108], and SSGs can be used to further classify the symmetry conditions for AHE to exist.

In conclusion, the vast number of SSGs we enumerated systematically in the work greatly enlarge the symmetries that could be used for describing magnetic materials and their band structures and could promote research in related fields.

Note added. Recently, we became aware of parallel studies conducted by Song's group and Liu's group, which are documented in their works (see Refs. [93,94], respectively). These groups have also explored the enumeration and applications of SSGs, albeit through distinct methodologies. In Supplemental Material Sec. IX [81], we provide a comparative analysis of our results with those of Song's and Liu's groups. We also give a brief discussion on how to effectively map these different notational systems.

ACKNOWLEDGMENTS

---

[1] T. Hahn, *International Tables for Crystallography, Space-Group Symmetry*, International Tables for Crystallography (Wiley, New York, 2005).

[2] C. Bradley and A. Cracknell, *The Mathematical Theory of Symmetry in Solids: Representation Theory for Point Groups and Space Groups*, EBSCO ebook academic collection (Oxford University, New York, 2010).

[3] C. J. Bradley and B. L. Davies, *Magnetic groups and their corepresentations*, Rev. Mod. Phys. **40**, 359 (1968).

[4] R. Lifshitz, *Magnetic point groups and space groups*, arXiv:cond-mat/0406675.

[5] D. B. Litvin, *Magnetic Group Tables: 1-, 2- and 3-dimensional magnetic subperiodic groups and magnetic space groups*, https://www.iucr.org/publ/978-0-9553602-2-0.

[6] S. V. Gallego, J. M. Perez-Mato, L. Elcoro, E. S. Tasci, R. M. Hanson, K. Momma, M. I. Aroyo, and G. Madariaga, *MAGNDATA: Towards a database of magnetic structures. I. The commensurate case*, J. Appl. Crystallogr. **49**, 1750 (2016).

[7] J. González-Platas, N. A. Katcho, and J. Rodríguez-Carvajal, *Extension of Hall symbols of crystallographic space groups to magnetic space groups*, J. Appl. Crystallogr. **54**, 338 (2021).

[8] G.-B. Liu, Z. Zhang, Z.-M. Yu, and Y. Yao, *MSGCorep: A package for corepresentations of magnetic space groups*, Comput. Phys. Commun. **288**, 108722 (2023).

[9] W. F. Brinkman and R. J. Elliott, *Theory of spin-space groups*, Proc. R. Soc. A **294**, 343 (1966), https://www.jstor.org/stable/2415409.

[10] D. Litvin and W. Opechowski, *Spin groups*, Physica (Utrecht) **76**, 538 (1974).

[11] R.-J. Slager, A. Mesaros, V. Juričić, and J. Zaanen, *The space group classification of topological band-insulators*, Nat. Phys. **9**, 98 (2013).

[12] S. M. Young, S. Zaheer, J. C. Y. Teo, C. L. Kane, E. J. Mele, and A. M. Rappe, *Dirac semimetal in three dimensions*, Phys. Rev. Lett. **108**, 140405 (2012).

[13] B.-J. Yang and N. Nagaosa, *A strain-absorbing design for tissue–machine interfaces using a tunable adhesive gel*, Nat. Commun. **5**, 5898 (2014).

[14] C. Fang, Y. Chen, H.-Y. Kee, and L. Fu, *Topological nodal line semimetals with and without spin-orbital coupling*, Phys. Rev. B **92**, 081201(R) (2015).

[15] H. Watanabe, H. C. Po, M. P. Zaletel, and A. Vishwanath, *Filling-enforced gaplessness in band structures of the 230 space groups*, Phys. Rev. Lett. **117**, 096404 (2016).

[16] B. Bradlyn, J. Cano, Z. Wang, M. G. Vergniory, C. Felser, R. J. Cava, and B. A. Bernevig, *Beyond Dirac and Weyl fermions: Unconventional quasiparticles in conventional crystals*, Science **353**, aaf5037 (2016).

[17] J. Kruthoff, J. de Boer, J. van Wezel, C. L. Kane, and R.-J. Slager, *Topological classification of crystalline insulators through band structure combinatorics*, Phys. Rev. X **7**, 041069 (2017).

[18] B. Bradlyn, L. Elcoro, J. Cano, M. G. Vergniory, Z. Wang, C. Felser, M. I. Aroyo, and B. A. Bernevig, *Topological quantum chemistry*, Nature (London) **547**, 298 (2017).

[19] N. P. Armitage, E. J. Mele, and A. Vishwanath, *Weyl and Dirac semimetals in three-dimensional solids*, Rev. Mod. Phys. **90**, 015001 (2018).

[20] Z. Song, T. Zhang, and C. Fang, *Diagnosis for non-magnetic topological semimetals in the absence of spin-orbit coupling*, Phys. Rev. X **8**, 031069 (2018).

[21] T. Zhang, Y. Jiang, Z. Song, H. Huang, Y. He, Z. Fang, H. Weng, and C. Fang, *Catalogue of topological electronic materials*, Nature (London) **566**, 475 (2019).

[22] M. G. Vergniory, L. Elcoro, C. Felser, N. Regnault, B. A. Bernevig, and Z. Wang, *A complete catalogue of high-quality topological materials*, Nature (London) **566**, 480 (2019).

[23] F. Tang, H. C. Po, A. Vishwanath, and X. Wan, *Comprehensive search for topological materials using symmetry indicators*, Nature (London) **566**, 486 (2019).

[24] J. Cano and B. Bradlyn, *Band representations and topological quantum chemistry*, Annu. Rev. Condens. Matter Phys. **12**, 225C246 (2021).

[25] Z. Song, T. Zhang, Z. Fang, and C. Fang, *Quantitative mappings between symmetry and topology in solids*, Nat. Commun. **9**, 3530 (2018).

[26] Z. Song, C. Fang, and Y. Qi, *Real-space recipes for general topological crystalline states*, Nat. Commun. **11**, 4197 (2020).

[27] J. Yang, Z.-X. Liu, and C. Fang, *Unlocking of time reversal, space-time inversion and rotation invariants in magnetic materials*, arXiv:2009.07864.

[28] P. Tang, Q. Zhou, G. Xu, and S.-C. Zhang, *Dirac fermions in an antiferromagnetic semimetal*, Nat. Phys. **12**, 1100 (2016).

[29] L. Liang and Y. Yu, *Semimetal with both Rarita-Schwinger-Weyl and Weyl excitations*, Phys. Rev. B **93**, 045113 (2016).

[30] H. Watanabe, H. C. Po, and A. Vishwanath, *Structure and topology of band structures in the 1651 magnetic space groups*, Sci. Adv. **4**, aat8685 (2018).

[31] G. Hua, S. Nie, Z. Song, R. Yu, G. Xu, and K. Yao, *Dirac semimetal in type-IV magnetic space groups*, Phys. Rev. B **98**, 201116(R) (2018).

[32] R. M. Geilhufe, F. Guinea, and V. Juričić, *Hund nodal line semimetals: The case of a twisted magnetic phase in the double-exchange model*, Phys. Rev. B **99**, 020404(R) (2019).

[33] J. Cano, B. Bradlyn, and M. G. Vergniory, *Multifold nodal points in magnetic materials*, APL Mater. **7**, 101125 (2019).

[34] Y. Xu, L. Elcoro, Z.-D. Song, B. J. Wieder, M. G. Vergniory, N. Regnault, Y. Chen, C. Felser, and B. A. Bernevig, *High-throughput calculations of magnetic topological materials*, Nature (London) **586**, 702 (2020).

[35] A. Bouhon, G. F. Lange, and R.-J. Slager, *Topological correspondence between magnetic space group representations and subdimensions*, Phys. Rev. B **103**, 245127 (2021).

[36] J. Yang, C. Fang, and Z.-X. Liu, *Symmetry-protected nodal points and nodal lines in magnetic materials*, Phys. Rev. B **103**, 245141 (2021).

[37] F. Tang and X. Wan, *Exhaustive construction of effective models in 1651 magnetic space groups*, Phys. Rev. B **104**, 085137 (2021).

[38] Y. Jiang, Z. Fang, and C. Fang, *A* **k** · **p** *effective Hamiltonian generator*, Chin. Phys. Lett. **38**, 077104 (2021).

[39] L. Elcoro, B. J. Wieder, Z. Song, Y. Xu, B. Bradlyn, and B. A. Bernevig, *Magnetic topological quantum chemistry*, Nat. Commun. **12**, 5965 (2021).

[40] G.-B. Liu, Z. Zhang, Z.-M. Yu, S. A. Yang, and Y. Yao, *Systematic investigation of emergent particles in type-III magnetic space groups*, Phys. Rev. B **105**, 085117 (2022).

[41] Z. Zhang, G.-B. Liu, Z.-M. Yu, S. A. Yang, and Y. Yao, *Encyclopedia of emergent particles in type-IV magnetic space groups*, Phys. Rev. B **105**, 104426 (2022).

[42] P. M. Lenggenhager, X. Liu, T. Neupert, and T. Bzdušek, *Triple nodal points characterized by their nodal-line structure in all magnetic space groups*, Phys. Rev. B **106**, 085128 (2022).

[43] F. Tang and X. Wan, *Complete classification of band nodal structures and massless excitations*, Phys. Rev. B **105**, 155156 (2022).

[44] B. Peng, Y. Jiang, Z. Fang, H. Weng, and C. Fang, *Topological classification and diagnosis in magnetically ordered electronic materials*, Phys. Rev. B **105**, 235138 (2022).

[45] B. A. Bernevig, C. Felser, and H. Beidenkopf, *Progress and prospects in magnetic topological materials*, Nature (London) **603**, 41 (2022).

[46] D. Fan, X. Wan, and F. Tang, *All hourglass bosonic excitations in the 1651 magnetic space groups and 528 magnetic layer groups*, Phys. Rev. Mater. **6**, 124201 (2022).

[47] J. Yang, Z.-X. Liu, and C. Fang, *Symmetry invariants in magnetically ordered systems having weak spin-orbit coupling*, arXiv:2105.12738.

[48] P. Liu, J. Li, J. Han, X. Wan, and Q. Liu, *Spin-group symmetry in magnetic materials with negligible spin-orbit coupling*, Phys. Rev. X **12**, 021016 (2022).

[49] A. Corticelli, R. Moessner, and P. A. McClarty, *Spin-space groups and magnon band topology*, Phys. Rev. B **105**, 064430 (2022).

[50] D. B. Litvin, *Spin point groups*, Acta Crystallogr. Sect. A **33**, 279 (1977).

[51] L. Šmejkal, J. Sinova, and T. Jungwirth, *Beyond conventional ferromagnetism and antiferromagnetism: A phase with nonrelativistic spin and crystal rotation symmetry*, Phys. Rev. X **12**, 031042 (2022).

[52] L. Šmejkal, J. Sinova, and T. Jungwirth, *Emerging research landscape of altermagnetism*, Phys. Rev. X **12**, 040501 (2022).

[53] I. Mazin, *Editorial: Altermagnetism—a new punch line of fundamental magnetism*, Phys. Rev. X **12**, 040002 (2022).

[54] S. Hayami, Y. Yanagi, and H. Kusunose, *Momentum-dependent spin splitting by collinear antiferromagnetic ordering*, J. Phys. Soc. Jpn. **88,** 123702 (2019).

[55] S. Hayami, Y. Yanagi, and H. Kusunose, *Bottom-up design of spin-split and reshaped electronic band structures in antiferromagnets without spin-orbit coupling: Procedure on the basis of augmented multipoles*, Phys. Rev. B **102,** 144441 (2020).

[56] H. Reichlová, R. L. Seeger, R. González-Hernández, I. Kounta, R. Schlitz, D. Kriegner, P. Ritzinger, M. Lammel, M. Leiviskä, V. Petříček *et al.*, *Macroscopic time reversal symmetry breaking by staggered spin-momentum interaction*, arXiv:2012.15651.

[57] Z. Feng, X. Zhou, L. Šmejkal, L. Wu, Z. Zhu, H. Guo, R. González-Hernández, X. Wang, H. Yan, P. Qin *et al.*, *An anomalous Hall effect in altermagnetic ruthenium dioxide*, Nat. Electron. **5,** 735 (2022).

[58] A. Bose, N. J. Schreiber, R. Jain, D.-F. Shao, H. P. Nair, J. Sun, X. S. Zhang, D. A. Muller, E. Y. Tsymbal, D. G. Schlom, and D. C. Ralph, *Tilted spin current generated by the collinear antiferromagnet ruthenium dioxide*, Nat. Electron. **5,** 267 (2022).

[59] H. Bai, L. Han, X. Y. Feng, Y. J. Zhou, R. X. Su, Q. Wang, L. Y. Liao, W. X. Zhu, X. Z. Chen, F. Pan, X. L. Fan, and C. Song, *Observation of spin splitting torque in a collinear antiferromagnet* RuO_2, Phys. Rev. Lett. **128,** 197202 (2022).

[60] S. Karube, T. Tanaka, D. Sugawara, N. Kadoguchi, M. Kohda, and J. Nitta, *Observation of spin-splitter torque in collinear antiferromagnetic* RuO_2, Phys. Rev. Lett. **129,** 137201 (2022).

[61] L. Šmejkal, R. González-Hernández, T. Jungwirth, and J. Sinova, *Crystal time-reversal symmetry breaking and spontaneous Hall effect in collinear antiferromagnets*, Sci. Adv. **6,** eaaz8809 (2020).

[62] R. González-Hernández, L. Šmejkal, K. Výborný, Y. Yahagi, J. Sinova, T. Jungwirth, and J. Železný, *Efficient electrical spin splitter based on nonrelativistic collinear antiferromagnetism*, Phys. Rev. Lett. **126,** 127701 (2021).

[63] R. D. Gonzalez Betancourt, J. Zubáč, R. Gonzalez-Hernandez, K. Geishendorf, Z. Šobáň, G. Springholz, K. Olejník, L. Šmejkal, J. Sinova, T. Jungwirth *et al.*, *Spontaneous anomalous Hall effect arising from an unconventional compensated magnetic phase in a semiconductor*, Phys. Rev. Lett. **130,** 036702 (2023).

[64] I. I. Mazin, *Altermagnetism in MnTe: Origin, predicted manifestations, and routes to detwinning*, Phys. Rev. B **107,** L100418 (2023).

[65] A. Hariki, T. Yamaguchi, D. Kriegner, K. Edmonds, P. Wadley, S. Dhesi, G. Springholz, L. Šmejkal, K. Výborný, T. Jungwirth *et al.*, *X-ray magnetic circular dichroism in altermagnetic* α-MnTe, Phys. Rev. Lett. **132,** 176701 (2024).

[66] M. Papaj, *Andreev reflection at the altermagnet-superconductor interface*, Phys. Rev. B **108,** L060508 (2023).

[67] S. A. A. Ghorashi, T. L. Hughes, and J. Cano, *Altermagnetic routes to Majorana modes in zero net magnetization*, arXiv:2306.09413.

[68] C. R. W. Steward, R. M. Fernandes, and J. Schmalian, *Dynamic paramagnon-polarons in altermagnets*, Phys. Rev. B **108,** 144418 (2023).

[69] Y.-P. Zhu, X. Chen, X.-R. Liu, P. Liu, H. Zha, C. Hong, Z. Jiang, X.-M. Ma, Y.-J. Hao, W. Liu, M. Zeng, J. Ding, S. Mo, Z. Liu, M. Ye, D. Shen, R.-H. He, S. Qiao, Q. Liu, and C. Liu, *Observation of nonrelativistic plaid-like spin splitting in a noncoplanar antiferromagnet*, Nature (London) **626,** 523 (2024).

[70] P. Liu, A. Zhang, J. Han, and Q. Liu, *Chiral Dirac-like fermion in spin-orbit-free antiferromagnetic semimetals*, Innovation **3,** 100343 (2022).

[71] A. Zhang, K. Deng, J. Sheng, P. Liu, S. Kumar, K. Shimada, Z. Jiang, Z. Liu, D. Shen, J. Li *et al.*, *Chiral Dirac fermion in a collinear antiferromagnet*, Chin. Phys. Lett. **40,** 126101 (2023).

[72] L.-D. Yuan, Z. Wang, J.-W. Luo, and A. Zunger, *Prediction of low-Z collinear and noncollinear antiferromagnetic compounds having momentum-dependent spin splitting even without spin-orbit coupling*, Phys. Rev. Mater. **5,** 014409 (2021).

[73] P.-J. Guo, Y.-W. Wei, K. Liu, Z.-X. Liu, and Z.-Y. Lu, *Eightfold degenerate fermions in two dimensions*, Phys. Rev. Lett. **127,** 176401 (2021).

[74] P.-J. Guo, Z.-X. Liu, and Z.-Y. Lu, *Quantum anomalous Hall effect in collinear antiferromagnetism*, npj Comput. Mater. **9,** 70 (2023).

[75] *The spin-space group database*, https://cmpdc.iphy.ac.cn/ssg.

[76] M. I. Aroyo, J. M. Perez-Mato, C. Capillas, E. Kroumova, S. Ivantchev, G. Madariaga, A. Kirov, and H. Wondratschek, *Bilbao crystallographic server: I. Databases and crystallographic computing programs*, Z. Kristallogr.-Crystall. Mater. **221,** 15 (2006).

[77] M. I. Aroyo, A. Kirov, C. Capillas, J. Perez-Mato, and H. Wondratschek, *Bilbao crystallographic server. II. Representations of crystallographic point groups and space groups*, Acta Crystallogr. Sect. A **62,** 115 (2006).

[78] M. I. Aroyo, J. Perez-Mato, D. Orobengoa, E. Tasci, G. de la Flor, and A. Kirov, *Crystallography online: Bilbao crystallographic server*, Bulg. Chem. Commun. **43,** 183 (2011), https://bgcryst.com/symp10/proceeding/02_Aroyo_183-197.pdf.

[79] S. V. Gallego, J. M. Perez-Mato, L. Elcoro, E. S. Tasci, R. M. Hanson, M. I. Aroyo, and G. Madariaga, *MAGNDATA: towards a database of magnetic structures. II. The incommensurate case*, J. Appl. Crystallogr. **49,** 1941 (2016).

[80] Édouard Goursat, *Cours d'Analyse Mathématique* (Gauthier-Villars, Paris, 1921), Vol. 2. Chap. IX, pp. 123–126.

[81] See Supplemental Material at http://link.aps.org/supplemental/10.1103/PhysRevX.14.031039 for more algorithm details and results.

[82] *Translationengleiche* means "with the same translations," and *klassengleiche* means "of the same (crystal) class."

[83] S. Altmann and P. Herzig, *Point-Group Theory Tables*, Oxford Science Publications (Clarendon, New York, 1994).

[84] *Wolfram Research. Inc., Mathematica, Version 13.1*, Champaign, IL, 2022.

[85] A. Janner and T. Janssen, *Symmetry of incommensurate crystal phases. I. Commensurate basic structures*, Acta Crystallogr. Sect. A **36,** 399 (1980).

[86] S. Van Smaalen, *Incommensurate Crystallography* (Oxford University, New York, 2007), Vol. 21.

[87] J. Perez-Mato, J. Ribeiro, V. Petricek, and M. Aroyo, *Magnetic superspace groups and symmetry constraints in incommensurate magnetic phases*, J. Phys. Condens. Matter **24,** 163201 (2012).

[88] Y. Zhang, Y. Sun, H. Yang, J. Železný, S. P. P. Parkin, C. Felser, and B. Yan, *Strong anisotropic anomalous Hall effect and spin Hall effect in the chiral antiferromagnetic compounds* Mn_3X (X = Ge, Sn, Ga, Ir, Rh, and Pt), Phys. Rev. B **95,** 075128 (2017).

[89] H. Chen, Q. Niu, and A. H. MacDonald, *Anomalous Hall effect arising from noncollinear antiferromagnetism*, Phys. Rev. Lett. **112,** 017205 (2014).

[90] P. Brown, V. Nunez, F. Tasset, J. Forsyth, and P. Radhakrishna, *Determination of the magnetic structure of* Mn_3Sn *using generalized neutron polarization analysis*, J. Phys. Condens. Matter **2,** 9409 (1990).

[91] A. S. Sukhanov, S. Singh, L. Caron, T. Hansen, A. Hoser, V. Kumar, H. Borrmann, A. Fitch, P. Devi, K. Manna, C. Felser, and D. S. Inosov, *Gradual pressure-induced change in the magnetic structure of the noncollinear antiferromagnet* Mn_3Ge, Phys. Rev. B **97,** 214402 (2018).

[92] H. C. Po, A. Vishwanath, and H. Watanabe, *Symmetry-based indicators of band topology in the 230 space groups*, Nat. Commun. **8,** 50 (2017).

[93] J. Ren, X. Chen, Y. Zhu, Y. Yu, A. Zhang, J. Li, C. Li, and Q. Liu, preceding paper, *Enumeration and representation theory of spin space groups*, Phys. Rev. X **14,** 031038 (2024).

[94] Z. Xiao, J. Zhao, Y. Li, R. Shindou, and Z.-D. Song, this issue, *Spin-space groups: Full classification and applications*, Phys. Rev. X **14,** 031037 (2024).

[95] J.-Q. Chen, M.-J. Gao, and G.-Q. Ma, *The representation group and its application to space groups*, Rev. Mod. Phys. **57,** 211 (1985).

[96] Z.-Y. Yang, J. Yang, C. Fang, and Z.-X. Liu, *A Hamiltonian approach for obtaining irreducible projective representations and the $k \cdot p$ perturbation for anti-unitary symmetry groups*, J. Phys. A **54,** 265202 (2021).

[97] Y. He, Y. Jiang, T. Zhang, H. Huang, C. Fang, and Z. Jin, *SymTopo: An automatic tool for calculating topological properties of nonmagnetic crystalline materials*, Chin. Phys. B **28,** 087102 (2019).

[98] Z. Song, S.-J. Huang, Y. Qi, C. Fang, and M. Hermele, *Topological states from topological crystals*, Sci. Adv. **5,** eaax2007 (2019).

[99] R. S. K. Mong, A. M. Essin, and J. E. Moore, *Antiferromagnetic topological insulators*, Phys. Rev. B **81,** 245209 (2010).

[100] C. Fang, M. J. Gilbert, and B. A. Bernevig, *Topological insulators with commensurate antiferromagnetism*, Phys. Rev. B **88,** 085406 (2013).

[101] L. Fu, C. L. Kane, and E. J. Mele, *Topological insulators in three dimensions*, Phys. Rev. Lett. **98,** 106803 (2007).

[102] L. Fu and C. L. Kane, *Topological insulators with inversion symmetry*, Phys. Rev. B **76,** 045302 (2007).

[103] J. Rodríguez-Carvajal, *CEA/Saclay*, France **1045,** 132 (2001), https://cdifx.univ-rennes1.fr/fps/fp_rennes.pdf.

[104] A. Wills, *A new protocol for the determination of magnetic structures using simulated annealing and representational analysis (SARAh)*, Physica (Amsterdam) **276B**–**278B,** 680 (2000).

[105] J. Yang and Z.-X. Liu, *Irreducible projective representations and their physical applications*, J. Phys. A **51,** 025207 (2018).

[106] L. Šmejkal, A. H. MacDonald, J. Sinova, S. Nakatsuji, and T. Jungwirth, *Anomalous Hall antiferromagnets*, Nat. Rev. Mater. **7,** 482 (2022).

[107] M.-T. Suzuki, T. Koretsune, M. Ochi, and R. Arita, *Cluster multipole theory for anomalous Hall effect in antiferromagnets*, Phys. Rev. B **95,** 094406 (2017).

[108] R. Shindou and N. Nagaosa, *Orbital ferromagnetism and anomalous Hall effect in antiferromagnets on the distorted fcc lattice*, Phys. Rev. Lett. **87,** 116801 (2001).